Uncertainty Regions for Multi-Target Regression via Input-Dependent Conformal Calibration

Anonymous authors
Paper under double-blind review

Abstract

We consider the problem of provable and effective uncertainty quantification (UQ) for multi-target regression tasks where we need to predict multiple related target variables. This is important in many safety-critical applications in domains including healthcare, engineering, and finance. Conformal prediction (CP) is a promising framework for calibrating predictive models for UQ with guaranteed finite sample coverage. There is relatively less work on multi-target CP compared to single-target CP, and existing methods tend to produce large prediction regions that are not useful in real-world applications. This paper proposes a novel approach referred to as *Adaptive Prediction Regions (APR)* to produce provably smaller prediction regions by exploiting heterogeneity in the input data. APR is inspired by the principle behind localized CP for single-target Guan (2023) and extends it to multi-target settings. The key idea behind APR is to perform adaptive calibration by assigning differential weights to multi-dimensional calibration examples based on their similarity to a test input. We theoretically analyze APR and show that it (a) achieves finite-sample coverage guarantees; and (b) constructs smaller prediction regions. Our experiments on diverse real-world datasets with various numbers of targets show that APR outperforms existing methods by producing significantly smaller prediction regions (achieving up to 85.51% reduction in region area) over state-of-the-art multi-target CP methods.

1 Introduction

Many real-world applications across domains such as healthcare, engineering, and finance involve predicting multiple related target output variables (aka multi-target regression). For example, in Patient Monitoring using wearable devices, accurately predicting both heart rate and blood pressure is essential LaFreniere et al. (2016); Moseley & Linden (2006). Similarly, in engineering, predictive maintenance systems for industrial equipment rely on models that can jointly predict vibration levels, temperature, and operational efficiency to prevent costly failures Compare et al. (2020). Advances in machine learning have enabled us to develop predictive models with high accuracy for multi-target regression tasks. However, high-stakes applications such as healthcare require more than just accurate predictions; they demand trustworthy and theoretically sound uncertainty quantification to enable safe and reliable decision-making by clinicians. For example, a prediction/uncertainty region in the multi-dimensional space that covers the true multi-target output with high probability (e.g., 95%). Conformal prediction (CP) Vovk et al. (2005); Romano et al. (2019); Guan (2019); Angelopoulos & Bates (2021); Vazquez & Facelli (2022); Angelopoulos et al. (2023) is a promising framework for achieving such provable uncertainty quantification (UQ). CP relies on a calibration approach given a black-box predictor and user-specified coverage $1-\alpha$ (e.g., 95%) to construct prediction intervals and sets that contain the true output with probability $(1-\alpha)$ for regression and classification tasks, respectively. While localized conformal prediction (LCP) Guan (2023) provides a powerful theoretical framework for input-dependent calibration in the single-target setting, our work can be viewed as a multi-target, empirically grounded extension of this idea, showing that localized calibration remains effective and tractable on a broad suite of real-world multi-output regression tasks.

Much of the existing work on CP focuses on single-target regression, and there is little work on CP for multi-target regression tasks. A naive approach for multi-target tasks is to apply CP to each target output

independently, but it can result in highly conservative (aka large) prediction/uncertainty regions, as it doesn't exploit the existing correlations between multiple target variables. Directional Quantile Regression (DQR) approach leverages the correlations among target variables to avoid their unlikely combinations in the prediction region Boček & Šiman (2017); Charlier et al. (2020). The spherically-transformed DQR approach (henceforth SOTA) Feldman et al. (2023), currently the leading conformal prediction method for multi-target regression, leverages a conditional deep generative model to learn representations of the target variables and thereby enhance DQR. However, its main limitation is that the resulting prediction regions are excessively large, making them impractical for real-world use. In healthcare domain, for instance, compact prediction regions are essential since they enable clinicians to quickly determine whether a patient is within a healthy range or at risk, and to take timely medical action.

Motivated by this challenge, this paper asks the following question: *How can we produce provably small prediction regions satisfying the marginal coverage constraint for multi-target regression tasks?* To answer this question, we develop a novel approach referred to as *Adaptive Prediction Regions (APR)*. APR is inspired by the principle behind localized CP for single-target Guan (2023) and extends it to multi-target settings. The key idea behind APR is to exploit the heterogeneity in the conditional distribution of output given input to use a test-input conditioned quantile threshold to construct valid and small prediction regions. The effectiveness of this general idea depends on the specific localization mechanism which has not received attention. Additionally, to the best of our knowledge, localized CP method hasn't been empirically tested on real-world applications in both single-target and multi-target settings. In our work, we specify and empirically evaluate multiple instantiations of localization to address this gap in the CP literature.

To achieve this with guaranteed marginal coverage, particularly when using input-dependent weighting (APR-W), APR utilizes an $\tilde{\alpha}$-level adjustment Guan (2023) which is critical for restoring the validity of the localized quantiles. In contrast, existing multi-target CP methods such as DQR and its variants employ a uniform quantile threshold for all test inputs. We prove that APR achieves distribution-free and model-agnostic (invariant to the choice of the underlying multi-target regression method) marginal coverage guarantee. We also prove that under mild conditions on the quantiles, APR produces small prediction regions when compared to multi-target CP methods based on a uniform quantile threshold for all test inputs. Our comprehensive experiments on nine real-world datasets demonstrate that APR produces significantly smaller prediction regions (by up to 85.51% reduction) compared to state-of-the-art methods, and the results validate our theory.

Contributions. The key contribution of this paper is the development, theoretical analysis, and evaluation of the *Adaptive Prediction Regions (APR)* algorithm for multi-target regression tasks.

Specific contributions include:

- Development of the APR algorithm, which constructs valid and small prediction regions based on the idea of test input-conditioned quantile threshold: extending the framework of localized CP Guan (2023) to multi-target regression, including the $\tilde{\alpha}$-level adjustment necessary for maintaining the marginal coverage guarantee in the weighted localized setting.

- Theoretical analysis to show that APR achieves coverage guarantee and produces smaller prediction regions compared to using uniform threshold for all test inputs.

- Localized CP is developed for single-target setting and analyzed primarily at a theoretical level. Studying effective localization schemes and empirical evaluation on real-world applications has received less attention. Therefore, APR extends this idea to the multi-target setting, specifies multiple approaches for localization, and is validated on several real-world datasets.

- Empirical evaluation on diverse real-world datasets to demonstrate the efficacy of APR over state-of-the-art baseline methods. Our code is available in the following anonymous GitHub repository `https://anonymous.4open.science/r/apr-4C4C/` for review purposes.

2 Background and Problem Setup

Notations. Let $\mathcal{D}_{\text{tr}} = \{(X_i, Y_i)\}_{i=1}^{n}$ be a training dataset with n samples, where $X \in \mathcal{X} \subseteq \mathbb{R}^p$ and $Y \in \mathcal{Y} \subseteq \mathbb{R}^d$ are the input feature vector and output response vector defined on the input space $\mathcal{X}$ and output space $\mathcal{Y}$, respectively. We assume that all input-output pairs are independently drawn from an underlying distribution $\mathcal{P}$, i.e., $(X, Y) \sim \mathcal{P}$. Let $\mathcal{D}_{\text{cal}} = \{(X_i, Y_i)\}_{i=n+1}^{n+m}$ be a calibration data set with m samples and X_{test} be a test input feature vector with its corresponding response vector Y_{test}. Suppose $R_{\mathcal{Y}}(X) \subseteq \mathcal{Y}$ is a mapping to generate a region in output space $\mathcal{Y}$ given an input X.

Our goal is to construct trustworthy uncertainty regions (aka prediction regions) for multi-target regression tasks illustrated in Figure 1, so that they satisfy a conformal coverage guarantee. Specifically, we say a region-generating process $R_{\mathcal{Y}}(X)$ guarantees $(1-\alpha)$ coverage if the following inequality holds:

$$\mathbb{P}_{(X_{\text{test}}, Y_{\text{test}}) \sim \mathcal{P}}\{Y_{\text{test}} \in R_{\mathcal{Y}}(X_{\text{test}})\} \geq 1 - \alpha. \tag{1}$$

Throughout this paper, we omit the subscript $(X, Y) \sim \mathcal{P}$ of the probability $\mathbb{P}$ about where the randomness comes from, unless otherwise specified.

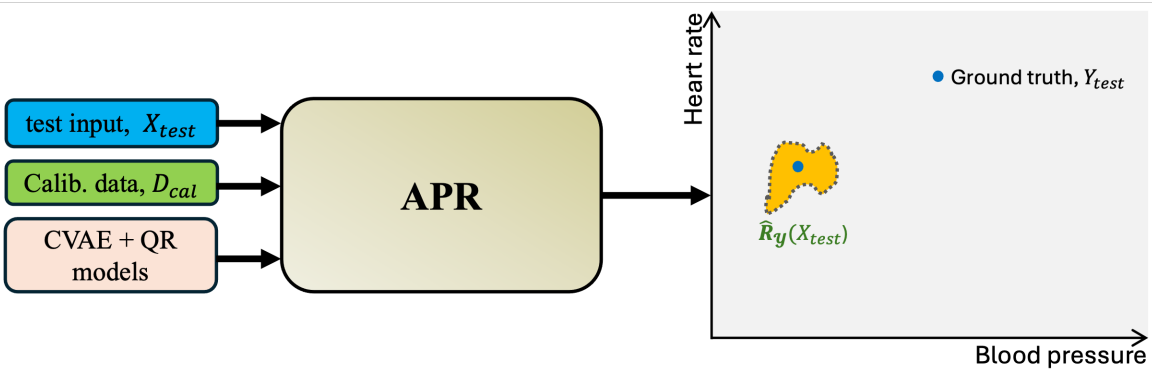

Figure 1: Illustration of the APR framework for constructing small prediction regions for a health application with two target variables (heart rate and blood pressure). Given a test input X_{test}, a calibration dataset D_{cal}, and pre-trained conditional variational autoencoder (CVAE) and multi-target quantile regression (QR) models, APR generates a compact prediction region ($\hat{R}_{\mathcal{Y}}(X_{\text{test}})$, shown in orange color) that is likely to contain the true target output (shown in blue) with a marginal coverage probability of $1-\alpha$ (say 95%).

Conformal Prediction is a general framework to provide rigorous guarantees for coverage in regression and classification tasks Vovk et al. (2005); Romano et al. (2019; 2020); Gibbs et al. (2023); Tibshirani et al. (2019). CP typically relies on a *non-conformity* scoring function which measures how different a data sample is from existing ones Vovk et al. (2005). For example, in single-target regression tasks, the absolute residual $|\hat{y} - y|$ due to a regression model is a commonly used definition for the non-conformity scoring function Romano et al. (2019), where $\hat{y}$ and y denote the predicted and true output, respectively. Moreover, the underlying regression model is trained and fixed during both calibration and testing stages.

Let $V : \mathcal{X} \times \mathcal{Y} \to \mathbb{R}$ denote a non-conformity scoring function.

For simplicity, we denote the non-conformity score for calibration sample $(X_j, Y_j) \in \mathcal{D}_{cal}$ by $V_j := V(X_j, Y_j)$.

Given a user-specified mis-coverage parameter α, CP methods typically compute an empirical quantile on the calibration dataset as follows:

$$\hat{Q}(\alpha) = \inf\left\{\tau : \frac{1}{m}\sum_{j \in \mathcal{D}_{cal}} \mathbb{1}\{V_j \leq \tau\} \geq 1 - \alpha\right\}. \tag{2}$$

For a test input X_{test}, we use this quantile as a threshold to selectively add candidate output responses into the prediction set:

$$\hat{\mathcal{C}}(X_{\text{test}}) = \{y \in \mathcal{Y} : V(X_{\text{test}}, y) \leq \hat{Q}(\alpha)\}.$$

It is a well-known result that if calibration data samples in $\mathcal{D}_{\text{cal}}$ and $(X_{\text{test}}, Y_{\text{test}})$ are exchangeable, then this CP procedure guarantees a marginal coverage Vovk et al. (2005):

$$\mathbb{P}\{Y_{\text{test}} \in \hat{\mathcal{C}}(X_{\text{test}})\} \geq 1 - \alpha.$$

The key difference between the above general coverage result and that in the multi-target regression setting in (1) is how the prediction set is constructed. In our problem setting, the region-generating function $R_{\mathcal{Y}}(X)$ builds the prediction region in the multi-dimensional output space (generalization of prediction interval in the single-target regression tasks). This is a significant challenge because the coverage in high-dimensional output space can be unnecessarily statistically inefficient, i.e., producing very large prediction regions to cover the true multi-target response.

Multi-target CP algorithm. We propose a wrapper-based solution that can use any existing multi-target method. Since we implemet our solution on top of the SOTA Feldman et al. (2023), we provide its key algorithmic steps for the sake of completeness.

SOTA begins by training a conditional variational autoencoder (CVAE) on the training dataset $\mathcal{D}_{\text{tr}}$. Specifically, we denote the CVAE by $(\mathcal{E}, \mathcal{D})$, where $\mathcal{E}$ and $\mathcal{D}$ are the encoder and decoder, respectively. Ideally, CVAE aims to fit the data to complete a two-way transform, by which it can reconstruct the conditional distribution $P(Y|X)$. The first transform is from $\mathcal{Y}$ to a latent space $\mathcal{Z} \subseteq \mathbb{R}^r$ by the encoder, i.e., to a transformed latent data point $Z_y = E(Y; X = x)$, where r is the dimensionality of the latent space and can be tuned as a hyper-parameter in practice. The ideal case is that all possible latent data points are drawn from a standard Normal distribution $Z_y \sim \mathcal{N}(0, 1)$. The second transform is from the latent space $\mathcal{Z}$ to the original response space $\mathcal{Y}$ by the decoder $\mathcal{D}(Z_y; X = x) = \hat{Y}$.

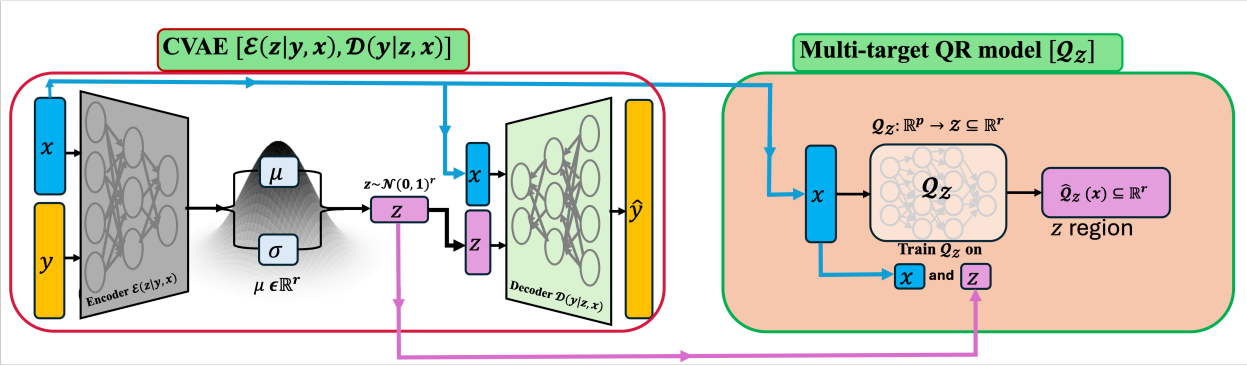

Figure 2: Overview of conditional variational autoencoder (CVAE) and multi-target quantile regression (QR) models training. The CVAE (on the left) and multi-target QR (on the right) models are trained on the training dataset to derive the encoder for mapping to the latent space $\mathcal{Z}$ and the decoder for reconstructing the original space $\mathcal{Y}$. The multi-target QR model is trained on the input (x) and latent target (z) to generate the base prediction region in the latent space $\mathcal{Z}$.

The goal of the encoder-decoder structure is to ensure that the reconstruction $\hat{Y}$ is equivalent to the true response Y in distribution, i.e., $\mathcal{D}(Z_y; X = x) \stackrel{d}{=} Y|X = x$.

Once the CVAE $(\mathcal{E}, \mathcal{D})$ is trained, proceed to train a standard directional quantile regression (DQR) in the latent space $\mathcal{Z}$. For an input X, this creates a convex region in $\mathcal{Z}$ (since DQR only generates convex regions), denoted by $R_{\mathcal{Z}}(X)$, which is then transformed using the decoder $\mathcal{D}$ to $\mathcal{Y}$ space. Particularly, we denote the

region in $\mathcal{Y}$ that is transformed from the latent space by $R_{\mathcal{Y}}(X) = \mathcal{D}(R_{\mathcal{Z}}(X))$, which serves as a base region in $\mathcal{Y}$.

DQR either provides over- or under-coverage in $\mathcal{Y}$, so it needs further calibration on (i) whether the coverage achieved by $R_{\mathcal{Y}}(X)$ is too large or too small, and (ii) how much it needs to adjust (shrink if too large, or expand if too small) the prediction region $R_{\mathcal{Y}}(X)$ in $\mathcal{Y}$ space. In the case of under-coverage, it uses the following non-conformity scoring function, calibration step, and region-generating process:

$$\begin{aligned} V_j^+ &= \min_{a \in R_{\mathcal{Y}}(X_j)} \text{dist}(a, Y_j), \forall j \in \mathcal{D}_{\text{cal}}, \\ \Rightarrow\ \gamma^+ &= \min\left\{\tau : \frac{1}{m}\sum_{j=n+1}^{n+m} \mathbb{1}[V_j^+ \leq \tau] \geq 1-\alpha\right\}, \\ \Rightarrow\ R_{\mathcal{Y}}^+(X_{\text{test}}) &= \left\{y \in \mathcal{Y} : \min_{a \in R_{\mathcal{Y}}(X_{\text{test}})} \text{dist}(a, y) \leq \gamma^+\right\} \end{aligned} \tag{3}$$

In the case of over-coverage, the non-conformity scoring function, calibration step, and prediction region can be defined as follows:

$$\begin{aligned} V_j^- &= \min_{a \in R_{\mathcal{Y}}^c(X_j)} \text{dist}(a, Y_j), \forall j \in \mathcal{D}_{\text{cal}}, \\ \Rightarrow\ \gamma^- &= \min\left\{\tau : \frac{1}{m}\sum_{j=n+1}^{n+m} \mathbb{1}[V_j^- \leq \tau] \leq \alpha\right\}, \\ \Rightarrow\ R_{\mathcal{Y}}^-(X_{\text{test}}) &= \left\{y \in \mathcal{Y} : \min_{a \in R_{\mathcal{Y}}(X_{\text{test}})} \text{dist}(a, y) \geq \gamma^-\right\}, \end{aligned}$$

where the $R_{\mathcal{Y}}^c(X_j) = \mathcal{Y} \backslash R_{\mathcal{Y}}(X_j)$ denotes the region that is not included by the quantile region $R_{\mathcal{Y}}(X_j)$. After either calibration step, the coverage in (1) is guaranteed to hold.

However, the calibration in SOTA does not consider the heterogeneity in the conditional probability distribution $P(Y|X)$. This is reflected in determining the quantile γ^+ and γ^-, both of which are defined in the marginal sense and are not adaptive to different realizations of test input X_{test}. The challenge of heterogeneous distribution $P(Y|X)$ is increasingly more important in the recent CP literature, especially when different kinds of conditional coverage notions have been proposed and investigated Gibbs et al. (2023); Vovk (2012); Ding et al. (2023). The main challenge to reduce the size of prediction regions is figuring out an algorithmic principle to capture the heterogeneity in the conditional distribution $P(Y|X)$ for multi-target conformal calibration.

Localized Conformal Prediction. While standard CP employs a single, global quantile threshold $\hat{Q}(\alpha)$ for all test inputs X_{test}, localized CP aims to compute a test input-specific quantile $Q(X_{\text{test}})$. One method to achieve this is to use weighted non-conformity scores. For a test input X_{test}, a localized quantile $\hat{Q}(X_{\text{test}}, \gamma)$ for a candidate confidence level γ is defined as:

$$\hat{Q}(X_{\text{test}}, \gamma) = \min\left\{\tau : \sum_{i \in \mathcal{D}_{\text{cal}}} w_i(X_{\text{test}}) \mathbb{1}\{V_i \leq \tau\} \geq \gamma\right\}, \tag{4}$$

where $w_i(X_{\text{test}}) \geq 0$ are weights such that $\sum_{i \in \mathcal{D}_{\text{cal}}} w_i(X_{\text{test}}) = 1$, and V_i are the non-conformity scores. A common issue with using $1-\alpha$ directly as γ is that it does not guarantee the marginal coverage ($\mathbb{P}(Y_{\text{test}} \in \hat{\mathcal{C}}(X_{\text{test}})) \geq 1-\alpha$) required by classic CP. To restore the marginal coverage guarantee in the weighted setting, Guan (2023) proposed learning a corrected confidence level $\tilde{\alpha}$ from the calibration set.

Specifically, for each calibration point X_i, let $\hat{q}_{X_i}(\gamma)$ be its localized quantile at level γ. Let Γ be the set of all cumulative weight values attainable from the weighted CDFs. The data-driven global correction level $\tilde{\alpha}$ is computed as:

$$\tilde{\alpha} = \min_{\gamma \in \Gamma}\left\{\gamma : \frac{1}{m}\sum_{i \in \mathcal{D}_{cal}} \mathbf{1}[V_i \leq \hat{q}_{X_i}(\gamma)] \ \geq\ 1-\alpha\right\}. \tag{5}$$

The prediction region is then constructed using the localized quantile at level $\tilde{\alpha}$ for the test point X_{test}: $\hat{\mathcal{C}}(X_{\text{test}}) = \{y \in \mathcal{Y} : V(X_{\text{test}}, y) \leq \hat{Q}(X_{\text{test}}, \tilde{\alpha})\}$. This $\tilde{\alpha}$-correction ensures the finite-sample marginal coverage guarantee.

The goal of this paper is to develop an adaptive multi-target CP algorithm that is statistically efficient to produce small prediction regions to guarantee the target marginal coverage.

3 Related Work

This section summarizes the related work on conformal prediction for regression tasks. Most of the existing CP work focuses on the simpler setting of single-task regression, and there is relatively little work on CP for the multi-target setting.

CP for single-target regression. Conformal prediction Vovk et al. (2005); Shafer & Vovk (2008); Angelopoulos & Bates (2021); Angelopoulos et al. (2023) leverages the assumption of data exchangeability to generate prediction intervals with guaranteed coverage levels for single-target regression tasks. The standard CP approach employs the distance to the conditional mean as the conformity scoring function for calibration. Conformalized quantile regression Romano et al. (2019) integrates CP with quantile regression Regression (2017); Romano et al. (2019); Koenker & Bassett Jr (1978) estimates to construct prediction intervals. Recent work Guan (2019); Lin et al. (2021); Guan (2023) has focused on improving the calibration process to reduce the size of prediction intervals without any theoretical guarantees. To reduce the size of prediction intervals when the output distribution is complex, a recent method Guha et al. (2024) considers a reduction from regression to classification and leverages recent advances in CP for classification Angelopoulos et al. (2020); Stutz et al. (2021); Huang et al. (2023); Ding et al. (2023). However, this approach is inherently limited to single-target regression and cannot be extended to multi-target regression due to the intricate nature of its multi-dimensional continuous target space. Furthermore, no existing work has explored CP in the context of joint multi-target classification.

CP for multi-target regression. A naive extension of single-target CP to the multi-target setting is by independently constructing prediction intervals for each output variable, which often results in overly conservative prediction regions Feldman et al. (2023). Extending CP to the multi-target regression setting poses significant challenges. There is relatively less work in this direction and no theoretical work on analyzing the size of prediction regions. Copula-based CP Messoudi et al. (2021) leverages copulas to provide valid coverage guarantees and reliable multi-target regions. However, it produces regions that are hyper-rectangular shaped, which are typically very large and difficult to interpret. Recent works Feldman et al. (2023); Dheur et al. (2025) used recent advances in representation learning to create smaller and arbitrarily shaped prediction regions that guarantee the desired coverage. It builds on the concept of directional quantile regression (DQR) Boček & Šiman (2017); Charlier et al. (2020) by mapping the target variable to a latent convex space, constructing quantile regions in the latent space using DQR, mapping the regions back to the original output space, and then calibrating the regions for coverage using the calibration set. However, this method constructs relatively large prediction regions, which are not useful in real-world applications because it uses a uniform quantile threshold for all testing inputs.

Probabilistic CP with approximate conditional validity. Plassier et al. Plassier et al. (2025) propose *probabilistic* conformal prediction sets that combine conformal inference with an estimate of the conditional distribution $P_{Y|X}$, and derive non-asymptotic guarantees for *approximate conditional validity* whose tightness explicitly depends on the conditional distribution estimation error (e.g., via discrepancies such as total variation). Our work is complementary in both goal and mechanism. While probabilistic CP constructs sets by thresholding probability mass under $\widehat{P}_{Y|X=x}$ (e.g., HPD/level-set type regions) to improve conditional behavior when accurate distribution estimation is available, we focus on *multi-target regression* and ask: given a strong predictive/generative model, how can we obtain *tighter* regions while preserving the standard distribution-free *finite-sample marginal coverage* guarantee? APR answers this by *localized calibration of nonconformity scores* using neighborhood-based weighting in either the input space or a learned representation (e.g., the CVAE latent space), together with the corrected global confidence level $\tilde{\alpha}$ to maintain

marginal validity under exchangeability. Consequently, APR can yield efficiency gains even when $\widehat{P}_{Y|X}$ is not accurate enough to support conditional-coverage bounds, since our validity guarantee does not rely on conditional density accuracy and the learned model affects efficiency rather than validity.

Theoretical comparison. In summary, Plassier et al. Plassier et al. (2025) obtain approximate conditional validity with bounds controlled by distribution-estimation error, whereas APR guarantees finite-sample marginal validity (via $\tilde{\alpha}$) and pursues efficiency through localized score calibration in input/latent space.

4 Adaptive Prediction Regions Algorithm

In this section, we describe our proposed algorithm, *Adaptive Prediction Regions (APR)*, in detail. Unlike the Naive and other multi-target CP methods, which apply a uniform quantile threshold across all test inputs to construct prediction regions, APR introduces a more adaptive approach. Specifically, APR utilizes a test-input-conditioned quantile threshold to create more efficient (i.e., smaller) prediction regions. Real-world problems often involve conditional distributions $P(Y|X)$ that are inherently heterogeneous. APR leverages this heterogeneity by defining a non-uniform quantile threshold that adapts uniquely to each test input. This adaptive threshold is determined based on the top-k weighted subset of calibration inputs that lie within a certain radius around the test input X_{test}, resulting in the construction of more adaptive prediction regions that better correspond to the true conditional distribution $P(Y|X)$.

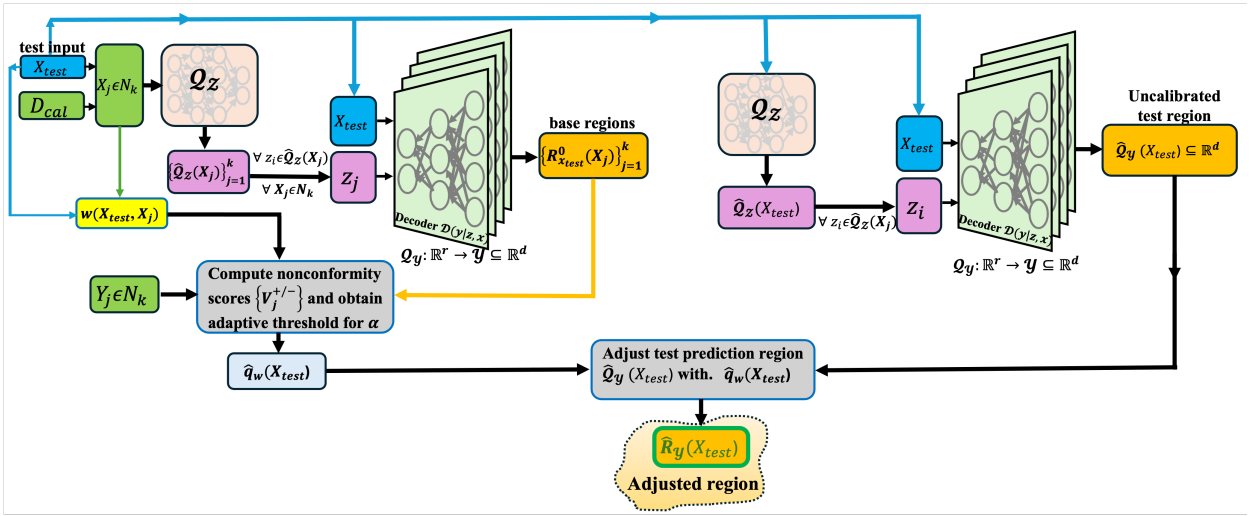

Figure 3: High-level overview of the APR algorithm illustrating the calibration and inference phases. The multi-target quantile regression model produces the initial (uncalibrated) prediction region, while the CVAE decoder maps the latent space back to the original target output space. During calibration and inference, the calibration dataset and weighting function are employed to construct a refined, smaller calibrated prediction region ($\hat{R}_{\mathcal{Y}}(X_{\text{test}})$) for the given test input X_{test}.

Following the procedure in Figure 2, we fit a CVAE, which comprises encoder $E(\cdot)$ and decoder $\mathcal{D}(\cdot)$, on $\mathcal{D}_{\text{tr}}$. The trained CVAE transforms the target vector Y into an r-dimensional standard normal distribution Z. The transformation of CVAE ensures that Z_i represents the expectation of $Y_i|X_i$. We then train a DQR model $Q_{\mathcal{Z}}$ on $\{(X_i, Z_i)\}_{i=1}^n : i \in \mathcal{D}_{tr}$ in the latent space, such that $Q_{\mathcal{Z}} : \mathbb{R}^p \to \mathcal{Z} \subseteq \mathbb{R}^r$ which constructs the base prediction region $Q_{\mathcal{Z}}(X) \subseteq \mathbb{R}^r$. Transforming $Q_{\mathcal{Z}}(X)$ back to the original $\mathcal{Y}$ space yields $Q_{\mathcal{Y}}(X) \subseteq \mathbb{R}^d$.

4.1 Adaptive Quantile Threshold via $\tilde{\alpha}$ Correction

Adaptive Calibration in APR. APR introduces a test-input conditioned quantile threshold $\hat{q}^{\text{APR}}_{X_{\text{test}}}$ to adapt the size of the prediction region based on local data density, enabling the construction of smaller regions in heterogeneous settings. The general form of the prediction region $\hat{R}_{\mathcal{Y}}(X_{\text{test}})$ for a test input X_{test} is:

$$\hat{R}_{\mathcal{Y}}(X_{\text{test}}) = \{y \in \mathcal{Y} : V(X_{\text{test}}, y) \leq \hat{q}^{\text{APR}}_{X_{\text{test}}}\} \tag{6}$$

where $V(\cdot, \cdot)$ is a non-conformity score (defined below as either V^+ or V^-) and $\hat{q}^{\text{APR}}_{X_{\text{test}}}$ is the final calibrated quantile threshold.

Localized Quantile Definition. The test-conditional quantile $\hat{q}_{X_{\text{test}}}(\gamma)$ for a candidate confidence level γ is computed using weighted non-conformity scores V_j from the calibration set $\mathcal{D}_{\text{cal}}$:

$$\hat{q}_{X_{\text{test}}}(\gamma) = \min\left\{\tau : \sum_{j \in \mathcal{D}_{\text{cal}}} w(X_{\text{test}}, X_j)\mathbb{1}\{V_j \leq \tau\} \geq \gamma\right\}, \tag{7}$$

where $w(X_{\text{test}}, X_j)$ is the weighting function (detailed below) that determines the influence of each calibration sample X_j based on its proximity to X_{test}.

Marginal Coverage Restoration via $\tilde{\alpha}$ Correction. For non-uniform weighting functions, using $\gamma = 1-\alpha$ in Equation (7) only guarantees conditional coverage. To ensure the desired finite-sample **marginal coverage** $\mathbb{P}\left[Y_{\text{test}} \in \hat{R}_{\mathcal{Y}}(X_{\text{test}})\right] \geq 1-\alpha$, APR employs the $\tilde{\alpha}$-level correction established in localized conformal prediction (LCP) Guan (2023). The corrected global confidence level $\tilde{\alpha}$ (where $\tilde{\alpha} \leq 1-\alpha$) is calculated using the calibration set $\mathcal{D}_{\text{cal}}$:

$$\tilde{\alpha} = \min_{\gamma \in \Gamma}\left\{\gamma : \frac{1}{m}\sum_{i \in \mathcal{D}_{cal}} \mathbf{1}[V_i \leq \hat{q}_{X_i}(\gamma)] \;\geq\; 1-\alpha\right\}, \tag{8}$$

where Γ is the set of attainable cumulative weight values from the localized weighted CDFs $\{\widehat{F}_{X_i}\}_{i \in \mathcal{D}_{cal}}$. The final calibrated threshold for the test input is then set as $\hat{q}^{\text{APR}}_{X_{\text{test}}} = \hat{q}_{X_{\text{test}}}(\tilde{\alpha})$.

Weighting Schemes (APR-U and APR-W). APR primarily uses k-Nearest Neighbor (k-NN) based localization. Let $N_k(X_{\text{test}})$ be the set of k nearest neighbors of X_{test} in $\mathcal{D}_{\text{cal}}$, where $\text{dist}(\cdot, \cdot)$ is a user-chosen metric on the representation vectors used for neighborhood search. In all experiments in this paper, we use the standard Euclidean (L_2) distance after feature standardization to form $N_k(X_{\text{test}})$. For APR-W, we use inverse-distance weights within $N_k(X_{\text{test}})$, i.e., $w(X_{\text{test}}, X_j) \propto 1/(\text{dist}(X_{\text{test}}, X_j) + \varepsilon)$ with a small $\varepsilon > 0$.

$$N_k(X_{\text{test}}) = \left\{X_j \in \mathcal{D}_{\text{cal}} : \sum_{X_k \in \mathcal{D}_{\text{cal}}} \mathbb{1}[\text{dist}(X_{\text{test}}, X_k) \leq \text{dist}(X_{\text{test}}, X_j)] \leq k\right\}$$

There are several ways of defining the weighting function $w(X_{\text{test}}, X_j)$:

(i) **Standard-uniform weights over $\mathcal{D}_{\text{cal}}$:**

$$w(X_{\text{test}}, X_j) = 1/m. \tag{9}$$

This reduces the adaptive calibration strategy of APR back to the standard calibration that is not adaptive to the realization of test input X_{test}.

(ii) **APR-U** (Uniform k-NN): Uniform weights are assigned to the k neighbors, which makes the localized weighted CDF depend only on the k neighbor scores; however, because the neighborhood depends on the realized test input, we still use the corrected global level $\tilde{\alpha}$ (Eq. 8) to guarantee finite-sample *marginal* coverage.

$$w(X_{\text{test}}, X_j) = 1/k \cdot \mathbb{1}[X_j \in N_k(X_{\text{test}})] \tag{10}$$

(iii) **APR-W** (Weighted k-NN): Inverse-distance weights are assigned to the k neighbors. This non-uniform weighting scheme is more adaptive but necessitates the full $\tilde{\alpha}$ computation (Equation 8) to guarantee marginal coverage.

$$w(X_{\text{test}}, X_j) = \frac{1/\text{dist}(X_{\text{test}}, X_j)}{\sum_{k \in N_k(X_{\text{test}})} 1/\text{dist}(X_{\text{test}}, X_k)} \cdot \mathbb{1}[X_j \in N_k(X_{\text{test}})] \tag{11}$$

(iv) **Ball-based Localizer**:

$$w(X_{\text{test}}, X_j) = \frac{\mathbb{1}[\phi(X_j) \in B(\phi(X_{\text{test}}))]}{\sum_{k \in \mathcal{D}_{cal}} \mathbb{1}[\phi(X_k) \in B(\phi(X_{\text{test}}))]} \tag{12}$$

where $\phi(X)$ is a feature mapping and $B(\cdot)$ is a Euclidean ball.

In this paper, we focus on the k-NN weighting functions: APR-U (Equation 10) and APR-W (Equation 11).

Initial Base Region. APR adapts a two-sided calibration approach to handle heterogeneity in the underlying predictor. This process starts by defining an initial base region $\mathbf{R}^{\mathbf{0}}_{\mathbf{X}_{\text{test}}}(X_j)$ for each calibration input $X_j \in N_k(X_{\text{test}})$ based on its uncalibrated region $Q_{\mathcal{Y}}(X_j)$ and a fixed initialization quantile $\hat{q}^{init}_{X_{\text{test}}}$:

$$\mathbf{R}^0_{X_{\text{test}}}(X_j) = \left\{ y \in \mathbb{R}^d : \min_{y_{in} \in Q_{\mathcal{Y}}(X_j)} \text{dist}(y_{in}, y) \leq \hat{q}^{init}_{X_{\text{test}}} \right\}, \tag{13}$$

where $Q_{\mathcal{Y}}(X_j) = \mathcal{D}(Q_{\mathcal{Z}}(X_j))$ is the uncalibrated region projected back to $\mathcal{Y}$. The $\hat{q}^{init}_{X_{\text{test}}}$ is an arbitrary initialization quantile (e.g., the $(1-\alpha)$ quantile of the distance between near points in $Q_{\mathcal{Y}}(X_{\text{test}})$) and $\text{dist}(\cdot)$ is the L_2 distance.

The initial coverage rate ($\mathbf{cov_{init}}$) for this base region is calculated over the k-NN set:

$$\mathbf{cov_{init}} = \frac{1}{k} \sum_{j \in N_k(X_{\text{test}})} \mathbb{1}[Y_j \in \mathbf{R}^{\mathbf{0}}_{\mathbf{X}_{\text{test}}}(X_j)]. \tag{14}$$

Calibration via Score Selection. Based on $\mathbf{cov_{init}}$, APR selects a non-conformity score (V^+ or V^-) and uses the $\tilde{\alpha}$ method to compute the final calibrated threshold $\hat{q}^{\text{APR}}_{X_{\text{test}}}$ (Equation 8 applied to the chosen score set).

Case (i): Under-Coverage ($\mathbf{cov_{init}} \leq 1-\alpha$). If the desired coverage is not achieved, we use the inward-distance score V^+ to expand the region. V^+ measures the distance from the true target Y_j to the closest point in the initial region $Q_{\mathcal{Y}}(X_j)$.

$$V_j^+ = \min_{y_{in} \in Q_{\mathcal{Y}}(X_j)} \text{dist}(y_{in}, Y_j), \forall j \in N_k(X_{\text{test}}). \tag{15}$$

The final calibrated prediction region $\hat{R}_{\mathcal{Y}}(X_{\text{test}})$ is constructed using the threshold $\hat{q}^{\text{APR}}_{X_{\text{test}}} = \hat{q}_{X_{\text{test}}}(\tilde{\alpha})$ computed on the set of $\{V_j^+\}$ scores:

$$\hat{R}_{\mathcal{Y}}(X_{\text{test}}) = \left\{ y \in \mathbb{R}^d : \min_{y_{in} \in Q_{\mathcal{Y}}(X_{\text{test}})} \text{dist}(y_{in}, y) \leq \hat{q}^{\text{APR}}_{X_{\text{test}}} \right\}. \tag{16}$$

This $\hat{q}^{\text{APR}}_{X_{\text{test}}}$ is the localized, $\tilde{\alpha}$-corrected version of the uncorrected $\hat{q}_w(X_{\text{test}})$ from the initial adaptive calibration idea.

Case (ii): Over-Coverage ($\mathbf{cov_{init}} > 1-\alpha$). If the initial region over-covers, we use the outward-distance score V^- to shrink the region. V^- measures the distance from the true target Y_j to the closest input in the **complement** region $Q^c_{\mathcal{Y}}(X_j)$, effectively calibrating the boundary of the region.

$$V_j^- = \min_{y_{in} \in Q^c_{\mathcal{Y}}(X_j)} \text{dist}(y_{in}, Y_j), \forall j \in N_k(X_{\text{test}}), \tag{17}$$

where $Q^c_{\mathcal{Y}}(X_j)$ is the complement of $Q_{\mathcal{Y}}(X_j)$. The final calibrated prediction region $\hat{R}_{\mathcal{Y}}(X_{\text{test}})$ is constructed using the threshold $\hat{q}^{\text{APR}}_{X_{\text{test}}} = \hat{q}_{X_{\text{test}}}(\tilde{\alpha})$ computed on the set of $\{V_j^-\}$ scores:

$$\hat{R}_{\mathcal{Y}}(X_{\text{test}}) = \left\{ y \in \mathbb{R}^d : \min_{y_{in} \in Q_{\mathcal{Y}}(X_{\text{test}})} \text{dist}(y_{in}, y) \leq \hat{q}^{\text{APR}}_{X_{\text{test}}} \right\}. \tag{18}$$

The key steps of the proposed APR algorithm are summarized in Algorithm 1 and illustrated in Figures 2 and **??**, offering a general overview.

Algorithm 1 Adaptive Prediction Regions (APR)

Input:
Data $\{(X_i, Y_i)\}_{i=1}^n \subseteq \mathbb{R}^p \times \mathbb{R}^d$**;** Multi-target QR algorithm $Q_{\mathcal{Z}}$**;**
VAE$(y : E, \mathcal{D}) = (E(z|y), \mathcal{D}(y|z))$**;** Test input X_{test}**;** error rate $\alpha \in (0, 1)$

Training CVAE and Multi-target-QR:
Randomly split the training data into two disjoint sets: training ($\mathcal{D}_{tr}$) and calibration ($\mathcal{D}_{cal}$).
Train VAE$(y : E, \mathcal{D})$ on $\mathcal{D}_{tr}$
Train $Q_{\mathcal{Z}}$ on $(X_i, E(z|Y_i))$, where $E(z|Y_i) = Z_i : i \in \mathcal{D}_{tr}$ and $Z_i \sim \mathcal{N}(0, 1)^r$.
$Q_{\mathcal{Z}}$ constructs the quantile region $Q_{\mathcal{Z}}(X) \subseteq \mathbb{R}^r$ in the latent space $\mathcal{Z}$.

APR calibration and Inference:
Obtain $N_k(X_{\text{test}}) \subseteq \mathcal{D}_{cal}$ and define $w(X_{\text{test}}, X_j)$ according to Eq (9) (11), (10) or (12)
Obtain base regions $\mathbf{R}^{\mathbf{0}}_{\mathbf{X}_{\text{test}}}(X_i), i \in N_k(X_{\text{test}})$ using Eq (13) and compute $\mathbf{cov_{init}}$ using Eq (14).
if $\mathbf{cov_{init}} \leq 1 - \alpha$: **then**
  – Compute scores $\{V_j^+\}$ from Eq (15) and construct region $\hat{R}_{\mathcal{Y}}(X_{\text{test}})$ using Eq (16)
else
  – Compute scores $\{V_j^-\}$ from Eq (17) and construct region $\hat{R}_{\mathcal{Y}}(X_{\text{test}})$ using Eq (18)
end if
Output: Prediction region, $\hat{R}_{\mathcal{Y}}(X_{\text{test}}) \subseteq \mathbb{R}^d$

4.2 Theoretical Analysis

In this section, we present our theoretical analysis for the coverage guarantee of APR and its improved predictive region efficiency over the baseline. Our analysis focuses on the weighting function choice of (10) in Algorithm 1, the test input-conditional calibration with the uniform weight on k-NN calibration samples for test input X_{test}. All our complete proofs can be found in Appendix A.1.

We start with the standard definition of exchangeability for *sequences* of random variables.

Definition 1. *A sequence of random variables $(Z_1, \ldots, Z_n)$ is exchangeable if for any permutation π of $\{1, \ldots, n\}$,*

$$(Z_1, \ldots, Z_n) \overset{d}{=} (Z_{\pi(1)}, \ldots, Z_{\pi(n)}).$$

In our setting, we apply this to the sequence of examples (X_i, Y_i) (calibration) together with the test example (X_{test}, Y_{test}).

Importantly, selecting a neighborhood (e.g., k-NN) based on the realized test input can break exchangeability within the selected subset. Therefore, rather than claiming exchangeability of the k-NN subset, our coverage guarantee follows the localized/weighted conformal framework using the corrected global confidence level $\tilde{\alpha}$ (Eq. 8), which restores finite-sample *marginal* validity (cf. localized conformal prediction).

Theorem 1. *(Finite-sample marginal coverage of APR with localization) Assume the calibration examples $\{(X_i, Y_i)\}_{i \in \mathcal{D}_{cal}}$ and the test example (X_{test}, Y_{test}) are exchangeable. Let the localized quantile $\hat{q}_X(\gamma)$ be defined via the (possibly sparse) weighting function $w(X, \cdot)$ and the corresponding weighted empirical CDF,*

and let $\tilde{\alpha}$ be chosen according to Eq. 8. Then the APR prediction region constructed using the calibrated threshold $\hat{q}^{\text{APR}}_{X_{test}} = \hat{q}_{X_{test}}(\tilde{\alpha})$ satisfies the distribution-free finite-sample marginal *coverage guarantee*

$$\mathbb{P}\{Y_{test} \in \hat{R}_{\mathcal{Y}}(X_{test})\} \geq 1 - \alpha.$$

Remark 1. The guarantee above is marginal (unconditional) coverage. The role of localization is to improve efficiency (smaller regions) under heterogeneity, while the corrected level $\tilde{\alpha}$ ensures finite-sample marginal validity under exchangeability.

Moreover, we highlight that the predictive region efficiency (aka area of prediction region) of different CP methods can be significantly distinct even though they guarantee the same coverage performance. Below, we show that under the concentrated condition of quantiles, our APR algorithm is more efficient in terms of the expected size of prediction regions when compared to the baseline multi-target CP method (SOTA in our study).

Definition 2. *(Preserving relative order of expected volume) Given two region-generating procedures conditional on X, i.e., $R_{\mathcal{Z}}(X), \tilde{R}_{\mathcal{Z}}(X) \subseteq \mathcal{Z}$ (latent space). A decoder $\mathcal{D}$ preserves the relative order of the expected volume if*

$$\begin{aligned} &\mathbb{E}_X[|(R_{\mathcal{Z}}(X)|] \leq \mathbb{E}_X[|(\tilde{R}_{\mathcal{Z}}(X)|] \\ \Rightarrow\ &\mathbb{E}_X[|D(R_{\mathcal{Z}}(X))|] \leq \mathbb{E}_X[|\mathcal{D}(\tilde{R}_{\mathcal{Z}}(X))|]. \end{aligned}$$

The preservation of the relative order of expected volume from $\mathcal{Z}$ to $\mathcal{Y}$ allows us to analyze the predictive efficiency. Based on the ideal CVAE, the latent variable in the latent space $\mathcal{Z}$ follows the multivariate Gaussian distribution $\mathcal{N}(0,1)^r$, which enables many statistical tools to understand how the density is distributed.

Theorem 2. *(Improved prediction region efficiency of APR) Suppose all calibration samples $(X_i, Y_i) \in \mathcal{D}_{cal}$ are exchangeable. Assume that the conditional VAE $(\mathcal{E}, \mathcal{D})$ and the underlying multi-target quantile regression are trained ideally. If the decoder $\mathcal{D}$ preserves the relative order of the expected volume when transforming regions from latent space $\mathcal{Z}$ to target space $\mathcal{Y}$, then the following holds:*

$$\mathbb{E}_X[|R_{\mathcal{Y}}(X)|] \leq \mathbb{E}_X[|R_{\mathcal{Y}}(X)|].$$

The above result demonstrates that the uniform k-NN weighting function improves the predictive efficiency of uncertainty regions while ensuring that the coverage is achieved. The improvement mainly comes from the concentration of Gaussian random variables in $\mathcal{Z}$ when the CVAE is ideally learned. We report the extensive empirical results below to support the theoretical insights.

Remark 2. **Assumptions and generality of Theorem 2.** Theorem 2 is an *efficiency* result (region size) and is not required for the marginal validity guarantee in Theorem 1. Its assumptions are stylized sufficient conditions that make the comparison analytically tractable. First, the "Gaussian latent" condition is motivated by the standard VAE prior $Z \sim \mathcal{N}(0, I)$; exact Gaussianity is idealized, but the same concentration intuition extends to approximately isotropic sub-Gaussian / log-concave latent distributions where high-probability mass concentrates. Second, "ideal" training of the underlying multi-target quantile model is used to simplify the geometry of the uncalibrated region in $\mathcal{Z}$ (approximately radial / symmetric), enabling clean volume comparisons. Third, the decoder assumption (preserving relative order of expected volume) is a sufficient regularity condition. For example, if the decoder $\mathcal{D}$ is approximately bi-Lipschitz on the relevant latent region, i.e., there exist constants $0 < c \leq C$ such that

$$c\|z_1 - z_2\| \leq \|\mathcal{D}(z_1) - \mathcal{D}(z_2)\| \leq C\|z_1 - z_2\|,$$

then volumes scale within constants: $c^d|R| \leq |\mathcal{D}(R)| \leq C^d|R|$, which preserves ordering up to multiplicative factors. In practice, these assumptions are not expected to hold exactly; rather, Theorem 2 provides a principled explanation of when localization yields smaller regions (heterogeneity + concentrated representations), which we corroborate empirically.

5 Experiments and Results

In this section, we present the experimental evaluation of the proposed APR method, comparing it against a naive baseline and the state-of-the-art SOTA method. We discuss the results in terms of the validity and size of the prediction region area (generally interpreted as hypervolume). For simplicity, we refer to this as "*area*" throughout the paper.

5.1 Experimental Setup

Datasets. We employed nine real-world datasets, consistent with those used in Romano et al. (2019); Feldman et al. (2023), and additional datasets spanning three broad application domains: 1) Healthcare, 2) Social sciences, and 3) Engineering. These datasets include Communities and Crime Dataset (Communities_2, Communities_3, Communities_4 for two, three, and four targets respectively) Redmond (2002), a dataset on physicochemical properties of protein tertiary structure (Bio) Rana (2013), House Sales in King County, USA (House) hou (2015), Blog feedback (Blog) Buza (2014), and the AI4I 2020 Predictive Maintenance Datasets (Maint._2, Maint._3, and Maint._4 for two, three, and four targets respectively) mis (2020). We additionally evaluate on the BIWI Kinect Head Pose dataset Fanelli et al. (2013) (denoted BIWI_2/, BIWI_3 depending on the number of pose targets), where each example is a face image and the targets are head-pose angles. Following the experimental protocol used in our prior draft, we featurize each image by flattening it to a 307,200-dimensional vector and then reduce the dimension to 3,072 via PCA before training. This ensures that the k-NN localization is performed on a low-dimensional, well-conditioned representation rather than in the raw pixel space. For datasets that originally featured 1-D targets (such as Bio, House, and Blog), we adapted them to include 2-D targets, following the approach in Feldman et al. (2023), making them appropriate for multi-target regression tasks. Further details on the number of targets and training, testing, validation, and calibration samples for each dataset are provided in Appendix A.2.

Configuration of algorithms and baselines. We compare two variants of our proposed APR method wrapped around SOTA, namely, `APR-U` (with uniform weights) and `APR-W` (with non-uniform weights), against baseline methods including `Naive` (independent CP for each target variable) and `SOTA` Feldman et al. (2023). Unless otherwise stated, we set the desired coverage level to $(1-\alpha) = 0.9$. We additionally evaluate $\alpha \in \{0.1, 0.05\}$ (i.e., 90% and 95% prediction regions) and report $\alpha = 0.05$ results in Appendix **??**. We focus on these two operating points because very small α (e.g., $\alpha < 0.01$) often yields extremely large multi-target regions that are difficult to visualize and compare meaningfully across datasets. For APR, we choose the neighborhood size k via a systematic sweep over $k \in [0.3m, 0.9m]$ (where $m = |\mathcal{D}_{\text{cal}}|$) and select the value that minimizes the prediction-region area; Table **??** reports the resulting average k values. We split the dataset as follows: 20% for testing, 16% for validation (used for early stopping), 12.8% for calibration, and the remaining 51.2% for training. This is achieved by first allocating 20% of the dataset to testing. Then, from the remaining data, 20% is set aside for validation, 20% of what remains after that is used for calibration, and the rest is used for training. To provide a common basis for comparison, we set the latent space $\mathcal{Z}$ for SOTA and APR to $r = 3$ and evaluated performance (coverage and prediction region area).

The Naive and SOTA methods were implemented using the official code available at `https://github.com/Shai128/mqr`. The experiments were run on a machine with Rocky Linux 8.10 (Green Obsidian) OS, an AMD EPYC 7573X 32-Core Processor, and two NVIDIA A40 GPUs (each with 46 GB of memory), using GPU Driver Version 555.42.02 and CUDA Version 12.5.

Evaluation methodology. We evaluate all methods using two metrics: 1) `coverage` and 2) `prediction region area`. Coverage is computed as the proportion of test samples for which the correct multi-target output is included within the predicted region. The prediction region area is calculated by discretizing the target output space $\mathcal{Y}$ into a grid and counting the number of grid points within the prediction region Feldman et al. (2023). We report coverage, region area, and the percentage reduction in region area relative to the Naive and SOTA baselines. When needed (e.g., in Figures 5–6), we normalize region areas by the smallest method so that the best method has relative area = 1.0. The results reported in this work average over 20 runs across all methods and datasets. Unless otherwise stated, we set the desired coverage level to

Coverage Rate and Relative Region Area in the Target Space $\mathcal{Y}$ for $\alpha = 0.1$

Dataset	Targets	Methods	Cov.	Relative Region Area ↓	Reduction(%) from Naive ↑	Reduction(%) from SOTA ↑
BIWI_2	2	Naive	0.92	1.74	–	–
		SOTA	0.91	1.18	32.42%	–
		APR-U	0.90	1.10	37.03%	6.81%
		APR-W	0.89	1.00	**42.61%**	**15.08%**
BIWI_3	3	Naive	0.93	3.06	–	–
		SOTA	0.92	1.28	57.95%	–
		APR-U	0.91	1.17	61.63%	8.76%
		APR-W	0.90	1.00	**67.27%**	**22.17%**
Community_2	2	Naive	0.90	2.36	–	–
		SOTA	0.91	1.07	54.59%	–
		APR-U	0.89	1.01	57.28%	5.91%
		APR-W	0.89	1.00	**57.57%**	**6.55%**
Community_3	3	Naive	0.90	4.99	–	–
		SOTA	0.90	1.10	77.94%	–
		APR-U	0.91	1.02	79.65%	7.75%
		APR-W	0.90	1.00	**79.96%**	**9.18%**
Community_4	4	Naive	0.90	11.60	–	–
		SOTA	0.91	1.16	90.02%	–
		APR-U	0.90	1.03	91.16%	11.37%
		APR-W	0.90	1.00	**91.38%**	**13.56%**
Bio	2	Naive	0.90	1.17	–	–
		SOTA	0.90	1.00	**14.33%**	–
		APR-U	0.90	1.01	13.60%	-0.86%
		APR-W	0.90	1.01	13.70%	-0.74%
House	2	Naive	0.90	1.18	–	–
		SOTA	0.90	1.04	11.52%	–
		APR-U	0.89	1.00	14.91%	3.83%
		APR-W	0.89	1.00	**15.05%**	**3.98%**
Blog	2	Naive	0.90	1.13	–	–
		SOTA	0.90	1.20	-5.98%	–
		APR-U	0.87	1.01	10.74%	15.78%
		APR-W	0.87	1.00	**11.73%**	**16.71%**
Maint._2	2	Naive	0.90	22.03	–	–
		SOTA	0.99	6.96	68.41%	–
		APR-U	0.86	1.00	**95.46%**	**85.63%**
		APR-W	0.95	1.01	95.42%	85.51%
Maint._3	3	Naive	0.91	4.87e2	–	–
		SOTA	0.98	1.44	99.70%	–
		APR-U	0.88	1.17	99.76%	18.87%
		APR-W	0.94	1.00	**99.79%**	**30.56%**
Maint._4	4	Naive	0.91	1.24e4	–	–
		SOTA	0.98	1.39	99.99%	–
		APR-U	0.98	1.00	99.99%	28.20%
		APR-W	0.87	1.00	**99.99%**	**28.12%**

Table 1: Coverage rates, relative region size, and reduction in region area size of APR relative to SOTA method in target space $\mathcal{Y}$ presented for nine datasets with multiple targets. Results for each dataset are averaged over 20 experimental runs with standard errors provided. Detailed raw experimental data and standard errors are provided in Appendix A.3.

$(1-\alpha) = 0.9$ and also report results for $\alpha \in \{0.1, 0.05\}$. We select the hyperparameter value λ using validation data. To choose k for the test input-conditioned quantile threshold in APR, we performed a systematic search between 30% and 90% of the calibration set, selecting the k value that provides the smallest region size in

Coverage Rate and Relative Region Area in the Target Space $\mathcal{Y}$ for $\alpha = 0.05$

Dataset	Targets	Methods	Cov.	Relative Region Area ↓	Reduction(%) from Naive ↑	Reduction(%) from SOTA ↑
BIWI_2	2	Naive	0.97	2.60	–	–
		SOTA	0.96	1.25	51.86%	–
		APR-U	0.94	1.08	58.42%	13.63%
		APR-W	0.93	1.00	**61.54%**	**20.10%**
BIWI_3	3	Naive	0.96	5.11	–	–
		SOTA	0.96	1.24	75.81%	–
		APR-U	0.95	1.18	76.98%	4.84%
		APR-W	0.94	1.00	**80.43%**	**19.08%**
Blog	2	Naive	0.95	1.34	–	–
		SOTA	0.96	1.14	14.94%	–
		APR-U	0.93	1.01	24.43%	11.16%
		APR-W	0.93	1.00	**25.24%**	**12.11%**
Bio	2	Naive	0.94	1.22	–	–
		SOTA	0.95	1.02	16.74%	–
		APR-U	0.94	1.00	17.86%	1.35%
		APR-W	0.95	1.00	**17.98%**	**1.49%**
Community_3	3	Naive	0.96	6.36	–	–
		SOTA	0.96	1.14	82.11%	–
		APR-U	0.95	1.02	84.02%	10.70%
		APR-W	0.95	1.00	**84.28%**	**12.15%**
Community_4	4	Naive	0.95	13.72	–	–
		SOTA	0.96	1.12	91.86%	–
		APR-U	0.95	1.03	92.53%	8.19%
		APR-W	0.95	1.00	**92.71%**	**10.45%**
Community_2	2	Naive	0.96	2.82	–	–
		SOTA	0.96	1.08	61.70%	–
		APR-U	0.95	1.01	64.26%	6.68%
		APR-W	0.95	1.00	**64.55%**	**7.42%**
House	2	Naive	0.95	1.30	–	–
		SOTA	0.95	1.07	17.58%	–
		APR-U	0.94	1.00	22.79%	6.33%
		APR-W	0.94	1.00	**22.96%**	**6.53%**
Maint._2	2	Naive	0.94	107.45	–	–
		SOTA	0.99	8.92	91.70%	–
		APR-U	0.92	1.00	99.07%	88.79%
		APR-W	0.97	1.07	**99.00%**	**87.98%**
Maint._3	3	Naive	0.95	3275.57	–	–
		SOTA	0.98	4.24	99.87%	–
		APR-U	0.93	1.00	99.97%	76.41%
		APR-W	0.97	1.00	**99.97%**	**76.35%**
Maint._4	4	Naive	0.95	210671.15	–	–
		SOTA	0.97	10.87	99.99%	–
		APR-U	0.93	1.13	100.00%	89.62%
		APR-W	0.99	1.00	**100.00%**	**90.80%**

Table 2: Coverage rates, relative area, and reduction in region size of APR relative to SOTA in $\mathcal{Y}$.

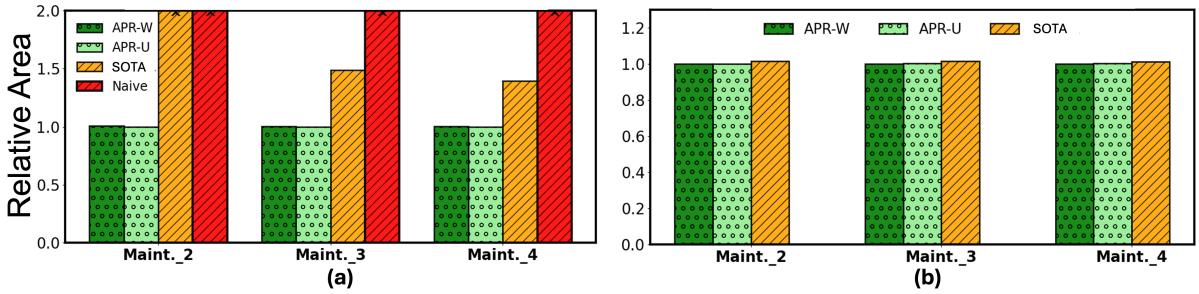

Figure 4: Relative region areas for Maintenance datasets. **a)** shows the relative region areas for APR, SOTA, and Naive methods in the target space $\mathcal{Y}$, while **b)** shows the areas for APR and SOTA methods in the latent space $\mathcal{Z}$ over 20 runs. The results show that in both $\mathcal{Y}$ and $\mathcal{Z}$ spaces, APR-based methods produce the smallest region (with relative area = 1), more prominent in our target space of interest $\mathcal{Y}$.

the validation phase. We provide the average k value (as a percentage of the calibration set) used by APR across all datasets in Appendix A.2.

Coverage Rate and Relative Region Area in Latent Space $\mathcal{Z}$

Dataset	Targets	Methods	Cov.	Region Area ↓	Relative Region Area ↓	Reduction(%) from SOTA ↑
Community_2	2	SOTA	0.89	21354.32	1.03	–
		APR-U	0.89	20943.52	1.01	1.92%
		APR-W	0.89	20728.20	**1.00**	**2.93%**
Community_3	3	SOTA	0.92	19500.43	1.08	–
		APR-U	0.90	18288.69	1.01	6.21%
		APR-W	0.90	18107.41	**1.00**	**7.14%**
Community_4	4	SOTA	0.91	23378.38	1.09	–
		APR-U	0.93	21758.72	1.01	6.93%
		APR-W	0.93	21504.10	**1.00**	**8.02%**
Bio	2	SOTA	0.91	18869.40	1.07	–
		APR-U	0.89	17709.60	1.00	6.15%
		APR-W	0.89	17645.01	**1.00**	**6.49%**
House	2	SOTA	0.90	17013.68	1.06	–
		APR-U	0.88	16158.43	1.00	5.03%
		APR-W	0.88	16130.17	**1.00**	**5.19%**
Blog	2	SOTA	0.89	18363.30	1.03	–
		APR-U	0.89	18075.51	1.01	1.57%
		APR-W	0.88	17818.78	**1.00**	**2.97%**
Maint._2	2	SOTA	0.95	26836.81	1.00	–
		APR-U	0.94	26468.54	1.02	1.37%
		APR-W	0.94	26426.70	**1.00**	**1.53%**
Maint._3	3	SOTA	0.95	19941.66	1.02	–
		APR-U	0.96	19700.93	1.00	1.21%
		APR-W	0.96	19649.40	**1.00**	**1.47%**
Maint._4	4	SOTA	0.93	12832.50	1.01	–
		APR-U	0.93	12721.29	1.00	0.87%
		APR-W	0.93	12689.18	**1.00**	**1.12%**

Table 3: Coverage rates, relative region size, and reduction in region area size of APR relative to SOTA method in latent space $\mathcal{Z}$ presented for nine datasets with multiple targets. Results for each dataset are averaged over 20 experimental runs, with standard errors provided.

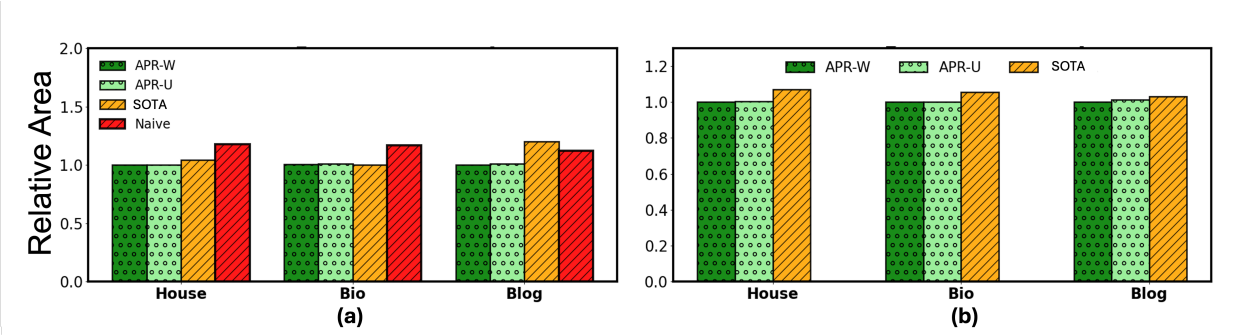

Figure 5: Relative region areas for House, Bio., and Blog datasets. **a)** shows the relative region areas for APR, SOTA, and Naive methods in the target space $\mathcal{Y}$, while **b)** shows the areas for APR and SOTA methods in the latent space $\mathcal{Z}$ over 20 runs. The results show that in both $\mathcal{Y}$ and $\mathcal{Z}$ spaces, APR-based methods generally produce the smallest region (with relative area = 1).

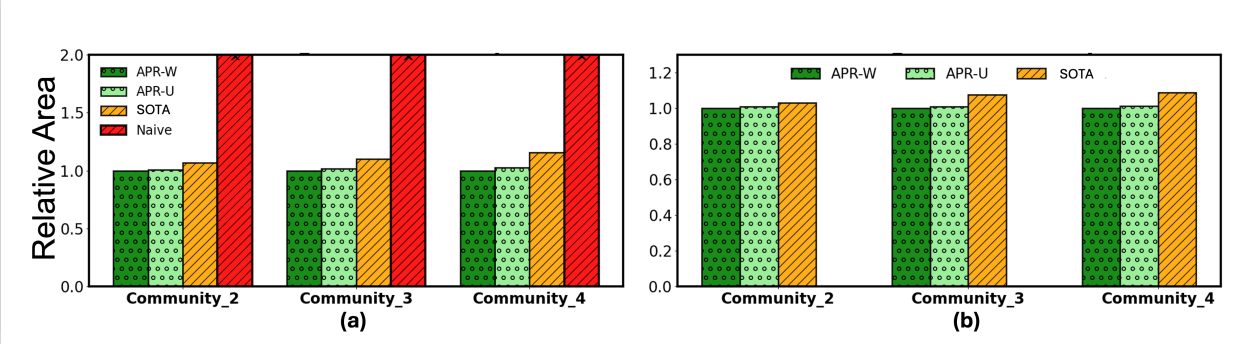

Figure 6: Relative region areas for Community and Crimes datasets. **a)** shows the relative region areas for APR, SOTA, and Naive methods in the target space $\mathcal{Y}$, while **b)** shows the areas for APR and SOTA methods in the latent space $\mathcal{Z}$ over 20 runs. The results show that in both $\mathcal{Y}$ and $\mathcal{Z}$ spaces, APR-based methods produce the smallest region (with relative area = 1).

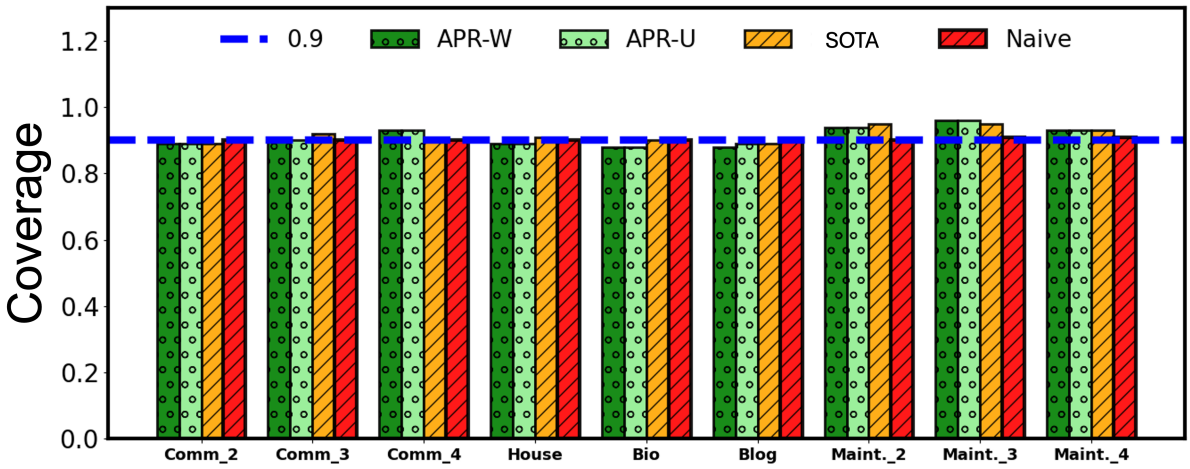

Figure 7: Empirical coverage for APR-based methods, SOTA, and Naive methods in target space $\mathcal{Y}$ (for Naive) and latent space $\mathcal{Z}$ over 20 runs. The results show that all methods generally achieve empirical coverage closer to the target level of 0.9.

Table 4: Final results on `clustered_close_1d` and `clustered_spread_1d` with test ratio 0.2 and calibration ratio 0.1. Reported values are averaged over 20 runs.

Dataset	Method	Area	Rel. area	Reduction vs. SOTA (%)
`clustered_close_1d`	SOTA	100.55	1.37	–
	APR	73.37	1.00	27.01
`clustered_spread_1d`	SOTA	274.60	1.66	–
	APR	165.02	**1.00**	**39.91**

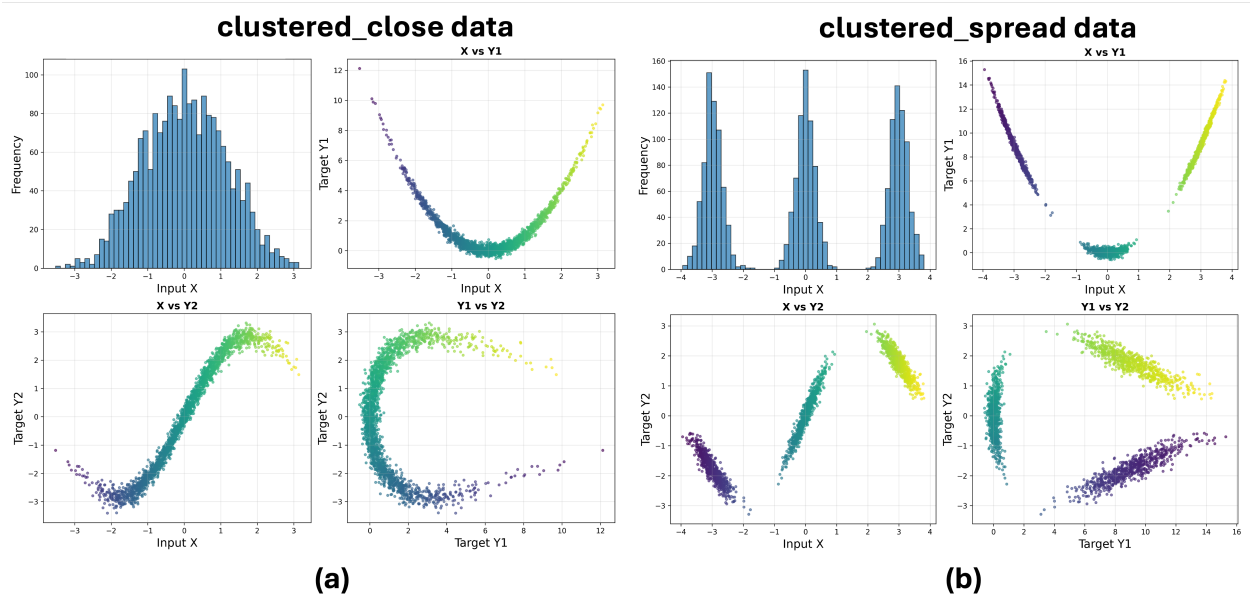

Figure 8: Synthetic clustered datasets used in our experiments. Panel (a) shows the `clustered_close_1d` data, where the one-dimensional covariate X is approximately unimodal and the two targets (Y_1, Y_2) vary smoothly with X. Panel (b) shows the `clustered_spread_1d` data, where X forms three well-separated clusters and the corresponding targets form distinct, cluster-specific patterns.The clear separation of clusters in `clustered_spread_1d` highlights the strong input-dependent heterogeneity that APR exploits.

5.2 Synthetic Data for Heterogeneity Analysis

We perform experiments on two synthetic datasets shown in Figure 8 to demonstrate the efficacy of APR in constructing smaller prediction regions when the conditional distribution $P(Y|X)$ is highly heterogeneous, particularly when the input data X exhibits clustering. Since APR uses localized calibration via k-NN weights, it can effectively restrict the calibration set to inputs that are most likely drawn from the same local data generation process as the test input X_{test}. This dramatically reduces the prediction region size compared to standard Conformal Prediction (CP) methods that calibrate globally.

Dataset Generation. Both synthetic datasets feature a 1-dimensional input $X \in \mathbb{R}$ and a 2-dimensional target $Y = (Y_1, Y_2) \in \mathbb{R}^2$. The data is generated from a mixture of $K = 3$ Gaussian clusters, where the cluster index K is sampled uniformly, $K \sim \text{Unif}\{1, 2, 3\}$.

For the `clustered_spread_1d` dataset, we use three well-separated clusters centered at -3, 0, and 3:

$$\mu_1^{(\text{spread})} = -3, \quad \mu_2^{(\text{spread})} = 0, \quad \mu_3^{(\text{spread})} = 3,$$
$$X \mid K = k \sim \mathcal{N}\big(\mu_k^{(\text{spread})}, \sigma^2_{\text{spread}}\big),$$

for a small variance $\sigma^2_{\text{spread}} > 0$ so that the three components are clearly separated on the real line. This scenario represents strong input clustering and heterogeneity.

For the `clustered_close_1d` dataset, we instead place the clusters closer together, with centers at -1, 0, and 1:

$$\mu_1^{(\text{close})} = -1, \quad \mu_2^{(\text{close})} = 0, \quad \mu_3^{(\text{close})} = 1,$$
$$X \mid K = k \sim \mathcal{N}\big(\mu_k^{(\text{close})}, \sigma^2_{\text{close}}\big),$$

with $\sigma^2_{\text{close}} > \sigma^2_{\text{spread}}$ so that the components overlap and the resulting clusters in X are much less clearly separated. This represents weak input clustering.

In both synthetic datasets, the two targets are generated from smooth nonlinear functions of X with independent Gaussian noise:

$$Y_1 = X + 0.5\sin(2X) + \varepsilon_1,$$
$$Y_2 = 0.5X^2 + \varepsilon_2,$$
$$\varepsilon_1, \varepsilon_2 \overset{\text{i.i.d.}}{\sim} \mathcal{N}(0, \sigma_y^2),$$

for some noise variance $\sigma_y^2 > 0$. Thus, the conditional distribution $P(Y \mid X)$ is smooth within each cluster, while the marginal distribution of X provides the main source of heterogeneity in the input space.

The results for the synthetic data experiments in Table4 show that APR substantially shrinks the prediction region area relative to SOTA, with the largest gains appearing on `clustered_spread_1d` where the input clusters are well separated. In this setting, APR can focus its kernel weights on calibration inputs drawn from the same cluster as the test input, yielding an area reduction of 39.91% compared to SOTA, whereas on `clustered_close_1d` the corresponding reduction is 27.01%. These synthetic experiments therefore provide a controlled illustration of APR's main advantage: when covariates form well-separated clusters, localized calibration around each test input produces markedly tighter multi-target prediction regions without compromising coverage.

5.3 Results and Discussion

Our experimental results are summarized in Tables 1 and 3. Table 1 shows the coverage, relative region area, and reduction in prediction region area with respect to Naive and SOTA, the state-of-the-art multi-target CP method in the target output space $\mathcal{Y}$. Table 3 shows similar results for the best-performing variant of APR (APR-W) and SOTA in the latent space $\mathcal{Z}$. Figure 7 shows the empirical coverages obtained by the Naive, SOTA, and APR-based methods. We summarize our key experimental findings below.

Empirical validation of the APR theory. We make the following observations from Tables 1 and 3, and Figures 4, 5, 6, and 7. **1)** APR methods generally achieve empirical marginal coverage on all datasets, validating Theorem 1. **2)** APR's coverage distribution in Figures 7 is closer to the target coverage level (0.9), providing robust empirical support for the theoretical guarantee in Theorem 1. **3)** Results in Tables 1 and 3 demonstrate the effectiveness of APR in reducing the prediction region area over the SOTA method, which uses a uniform threshold for all test inputs. **4)** Across both target space $\mathcal{Y}$ and latent space $\mathcal{Z}$, APR constructs smaller prediction regions than the baseline for all datasets, which empirically shows that the decoder preserved the relative order of the expected volume when transforming from $\mathcal{Z}$ to $\mathcal{Y}$ space as posited in Theorem 2.

APR-based methods vs. state-of-the-art. We make the following observations from Tables 1 and 3. **1)** All multi-target CP methods, including APR variants and SOTA, produce smaller prediction regions when compared to the Naive baseline. This result demonstrates the importance of joint reasoning by exploiting the correlations between target variables to construct prediction regions. **2)** APR-W variant with non-uniform weights for k-NN calibration examples performs better than APR-U in most cases. This result demonstrates the importance of distance-based non-uniform weighting. **3)** While all methods approximately achieve the nominal target coverage level, APR-based methods consistently produced significantly smaller and more adaptive prediction regions. When compared to the state-of-the-art SOTA method, APR achieves a maximum reduction of 85.51% in the prediction region area in the target output space $\mathcal{Y}$. This result

demonstrates the importance of the test input-conditional quantile threshold approach in reducing prediction region sizes. Further detailed experimental results and comparisons showcasing the efficacy of APR-based methods over baseline methods are provided in Appendix A.3.

6 Summary and Future Work

This paper studied a provable conformal prediction approach for multi-target regression tasks called Adaptive Prediction Regions (APR). APR relies on test input-conditioned quantile threshold to generate small and valid prediction regions that adapt to each test input. Our experiments on diverse real-world datasets demonstrate that APR significantly reduces the size of prediction regions over state-of-the-art methods. Future work includes conformal training for multi-target regression and deployment in healthcare applications.

7 Acknowledgments

This work was supported in part by USDA-NIFA funded AgAID Institute, the National Institutes of Health (NIH), and the National Science Foundation (NSF). The views expressed are those of the authors and do not reflect the official policy or position of the USDA-NIFA, NIH, or NSF.

References

House sales in king county, usa, 2015. https://www.kaggle.com/harlfoxem/housesalesprediction Accessed: August, 2024.

AI4I 2020 Predictive Maintenance Dataset. UCI Machine Learning Repository, 2020. https://doi.org/10.24432/C5HS5C Accessed: August, 2024.

Anastasios Angelopoulos, Stephen Bates, Jitendra Malik, and Michael I Jordan. Uncertainty sets for image classifiers using conformal prediction. *arXiv preprint arXiv:2009.14193*, 2020.

Anastasios N Angelopoulos and Stephen Bates. A gentle introduction to conformal prediction and distribution-free uncertainty quantification. *arXiv preprint arXiv:2107.07511*, 2021.

Anastasios N Angelopoulos, Stephen Bates, et al. Conformal prediction: A gentle introduction. *Foundations and Trends® in Machine Learning*, 16(4):494–591, 2023.

Pavel Boček and Miroslav Šiman. Directional quantile regression in r. *Kybernetika*, 53(3):480–492, 2017.

Krisztian Buza. BlogFeedback. UCI Machine Learning Repository, 2014. https://doi.org/10.24432/C58S3F Accessed: August, 2024.

Isabelle Charlier, Davy Paindaveine, and Jérôme Saracco. Multiple-output quantile regression through optimal quantization. *Scandinavian Journal of Statistics*, 47(1):250–278, 2020.

Michele Compare, Piero Baraldi, I Bani, Enrico Zio, and D McDonnell. Industrial equipment reliability estimation: A bayesian weibull regression model with covariate selection. *Reliability Engineering & System Safety*, 200:106891, 2020.

Victor Dheur, Matteo Fontana, Yorick Estievenart, Naomi Desobry, and Souhaib Ben Taieb. A unified comparative study with generalized conformity scores for multi-output conformal regression. *arXiv preprint arXiv:2501.10533*, 2025.

Tiffany Ding, Anastasios N Angelopoulos, Stephen Bates, Michael I Jordan, and Ryan J Tibshirani. Class-conditional conformal prediction with many classes. *arXiv preprint arXiv:2306.09335*, 2023.

Gabriele Fanelli, Matthias Dantone, Juergen Gall, Andrea Fossati, and Luc Van Gool. Random forests for real time 3d face analysis. *International Journal of Computer Vision (IJCV)*, 101(3):437–458, February 2013.

Shai Feldman, Stephen Bates, and Yaniv Romano. Calibrated multiple-output quantile regression with representation learning. *Journal of Machine Learning Research*, 24(24):1–48, 2023.

Isaac Gibbs, John J Cherian, and Emmanuel J Candès. Conformal prediction with conditional guarantees. *arXiv preprint arXiv:2305.12616*, 2023.

Leying Guan. Conformal prediction with localization. *arXiv preprint arXiv:1908.08558*, 2019.

Leying Guan. Localized conformal prediction: A generalized inference framework for conformal prediction. *Biometrika*, 110(1):33–50, 2023.

Etash Guha, Shlok Natarajan, Thomas Möllenhoff, Mohammad Emtiyaz Khan, and Eugene Ndiaye. Conformal prediction via regression-as-classification, 2024. URL `https://arxiv.org/abs/2404.08168`.

Jianguo Huang, Huajun Xi, Linjun Zhang, Huaxiu Yao, Yue Qiu, and Hongxin Wei. Conformal prediction for deep classifier via label ranking. *arXiv preprint arXiv:2310.06430*, 2023.

Roger Koenker and Gilbert Bassett Jr. Regression quantiles. *Econometrica: journal of the Econometric Society*, pp. 33–50, 1978.

Daniel LaFreniere, Farhana Zulkernine, David Barber, and Ken Martin. Using machine learning to predict hypertension from a clinical dataset. In *2016 IEEE symposium series on computational intelligence (SSCI)*, pp. 1–7. Ieee, 2016.

Zhen Lin, Shubhendu Trivedi, and Jimeng Sun. Locally valid and discriminative prediction intervals for deep learning models. In M. Ranzato, A. Beygelzimer, Y. Dauphin, P.S. Liang, and J. Wortman Vaughan (eds.), *Advances in Neural Information Processing Systems*, volume 34, pp. 8378–8391. Curran Associates, Inc., 2021. URL `https://proceedings.neurips.cc/paper_files/paper/2021/file/46c7cb50b373877fb2f8d5c4517bb969-Paper.pdf`.

Soundouss Messoudi, Sébastien Destercke, and Sylvain Rousseau. Copula-based conformal prediction for multi-target regression. *Pattern Recognition*, 120:108101, 2021.

Janine V Moseley and Wolfgang Linden. Predicting blood pressure and heart rate change with cardiovascular reactivity and recovery: results from 3-year and 10-year follow up. *Psychosomatic medicine*, 68(6):833–843, 2006.

Vincent Plassier, Alexander Fishkov, Mohsen Guizani, Maxim Panov, and Eric Moulines. Probabilistic conformal prediction with approximate conditional validity. In *International Conference on Learning Representations (ICLR)*, 2025.

Prashant Rana. Bio Physicochemical Properties of Protein Tertiary Structure. UCI Machine Learning Repository, 2013. DOI: https://doi.org/10.24432/C5QW3H Accessed: August, 2024.

Michael Redmond. Communities and Crime. UCI Machine Learning Repository, 2002. DOI: https://doi.org/10.24432/C53W3X.

Quantile Regression. *Handbook of quantile regression*. CRC Press: Boca Raton, FL, USA, 2017.

Yaniv Romano, Evan Patterson, and Emmanuel Candes. Conformalized quantile regression. *Advances in Neural Information Processing Systems*, 32, 2019.

Yaniv Romano, Matteo Sesia, and Emmanuel Candes. Classification with valid and adaptive coverage. *Advances in Neural Information Processing Systems*, 33:3581–3591, 2020.

Glenn Shafer and Vladimir Vovk. A tutorial on conformal prediction. *Journal of Machine Learning Research*, 9(3), 2008.

David Stutz, Ali Taylan Cemgil, Arnaud Doucet, et al. Learning optimal conformal classifiers. *arXiv preprint arXiv:2110.09192*, 2021.

Ryan J Tibshirani, Rina Foygel Barber, Emmanuel Candes, and Aaditya Ramdas. Conformal prediction under covariate shift. *Advances in neural information processing systems*, 32, 2019.

Janette Vazquez and Julio C Facelli. Conformal prediction in clinical medical sciences. *Journal of Healthcare Informatics Research*, 6(3):241–252, 2022.

Vladimir Vovk. Conditional validity of inductive conformal predictors. In *Asian conference on machine learning*, pp. 475–490. PMLR, 2012.

Vladimir Vovk, Alexander Gammerman, and Glenn Shafer. *Algorithmic learning in a random world*, volume 29. Springer, 2005.

A Appendix

A.1 Technical Proof

Theorem 1. *Assume the calibration examples $\{(X_i, Y_i)\}_{i\in\mathcal{D}_{cal}}$ and the test example (X_{test}, Y_{test}) are exchangeable. Let V_i denote the nonconformity score computed for (X_i, Y_i) (and similarly V_{test} for (X_{test}, Y_{test})). For any center X, define normalized weights*

$$\bar{w}_j(X) \;:=\; \frac{w(X, X_j)}{\sum_{\ell\in\mathcal{D}_{cal}} w(X, X_\ell)}, \qquad j \in \mathcal{D}_{cal},$$

and the weighted empirical CDF

$$\hat{F}_X(t) \;:=\; \sum_{j\in\mathcal{D}_{cal}} \bar{w}_j(X)\, \mathbf{1}\{V_j \le t\}.$$

Let the corresponding weighted γ-quantile be

$$\hat{q}_X(\gamma) \;:=\; \inf\{t : \hat{F}_X(t) \ge \gamma\}.$$

Choose the corrected global level $\tilde{\alpha}$ according to Eq. 8. Then the APR prediction region $\hat{R}_{\mathcal{Y}}(X_{test})$ constructed using $\hat{q}^{\mathrm{APR}}_{X_{test}} = \hat{q}_{X_{test}}(\tilde{\alpha})$ satisfies the distribution-free finite-sample marginal coverage guarantee

$$\mathbb{P}\{Y_{\text{test}} \in \hat{R}_{\mathcal{Y}}(X_{\text{test}})\} \ge 1 - \alpha.$$

Proof. The main subtlety is that localization uses weights $w(X_{\text{test}}, \cdot)$ (or a k-NN neighborhood) that depend on the realized test input X_{test}; thus, the subset of scores receiving nonzero weight is not, in general, an exchangeable subset. Hence, we do not rely on the exchangeability of the localized neighborhood. Instead, we follow the localized conformal prediction argument that restores finite-sample *marginal* validity via a corrected global confidence level.

For each calibration center X_i, define the (pseudo-test) inclusion indicator

$$A_i(\gamma) \;:=\; \mathbf{1}\{V_i \le \hat{q}_{X_i}(\gamma)\}, \qquad i \in \mathcal{D}_{cal}.$$

By construction of $\tilde{\alpha}$ (Eq. 8), we have

$$\frac{1}{m}\sum_{i\in\mathcal{D}_{cal}} A_i(\tilde{\alpha}) \;\ge\; 1 - \alpha, \qquad m := |\mathcal{D}_{cal}|. \tag{1}$$

Now define the corresponding test inclusion indicator

$$A_{\text{test}}(\tilde{\alpha}) \;:=\; \mathbf{1}\{V_{\text{test}} \le \hat{q}_{X_{\text{test}}}(\tilde{\alpha})\}. \tag{2}$$

Consider the augmented exchangeable $(m+1)$-tuple consisting of the m calibration examples and the test example. Exchangeability implies that the test index is uniformly distributed among the $(m+1)$ positions; therefore, the probability of inclusion for the held-out example is controlled by the average inclusion behavior under the same rule. In particular, the corrected-level choice yields

$$\mathbb{P}\{A_{\text{test}}(\tilde{\alpha}) = 1\} \;\ge\; 1 - \alpha, \quad \text{i.e., } \mathbb{P}\{V_{\text{test}} \le \hat{q}_{X_{\text{test}}}(\tilde{\alpha})\} \ge 1 - \alpha. \tag{3}$$

Finally, by definition of the APR prediction region,

$$A_{\text{test}}(\tilde{\alpha}) = 1 \iff Y_{\text{test}} \in \hat{R}_{\mathcal{Y}}(X_{\text{test}}). \tag{4}$$

Combining (3) and (4) proves $\mathbb{P}\{Y_{\text{test}} \in \hat{R}_{\mathcal{Y}}(X_{\text{test}})\} \ge 1 - \alpha$. □

Theorem 2. *Suppose all calibration samples $(X_i, Y_i) \in \mathcal{D}_{cal}$ are exchangeable. Assume that the conditional VAE $(\mathcal{E}, \mathcal{D})$ and the underlying multi-target quantile regression are trained ideally. If the decoder $\mathcal{D}$ preserves the relative order of the expected volume when transforming regions from latent space $\mathcal{Z}$ to target space $\mathcal{Y}$, then the following holds:*

$$\mathbb{E}_X[|R_{\mathcal{Y}}(X)|] \leq \mathbb{E}_X[|R_{\mathcal{Y}}(X)|].$$

Proof. Under the condition that the conditional VAE $(\mathcal{E}, \mathcal{D})$ is trained ideally such that $Z_y = \mathcal{E}(Y|X) \sim \mathcal{N}(0,1)^r$, where r is the dimensionality of the latent space. If the underlying multi-target quantile regression model is also trained ideally, then it has a threshold that is uniform in each direction in the $\mathcal{Z}$ space. The ideal training ensures that the latent representations are isotropic and standardized, making the calibrated region in $\mathcal{Z}$ a multi-dimensional ball (or hyper-sphere) centered at the mean. Thus, quantifying the volume of the calibrated region in $\mathcal{Z}$ space reduces to quantifying the radius of this ball, as the volume is $c \cdot v^r$ where c is a dimension-dependent constant and v is the radius. Since the decoder preserves the relative order of expected volumes and v^r is monotonic in v for $v > 0$, comparing the (expected) radii suffices to compare the (expected) volumes.

Now the question is how to quantify the radius produced by the two region-generating procedures $R_{\mathcal{Z}}(X)$ and $R_{\mathcal{Z}}(X)$. We establish this through the following lemmas and then combine them.

Lemma 1. *The radius v produced by $R_{\mathcal{Z}}(X)$ satisfies*

$$v \geq \sqrt{2\log(1/\alpha)}.$$

Proof. Given a Gaussian distribution $\mathcal{N}(0,1)$, the well-known tail bound for a single direction is:

$$P(X - \mathbb{E}[X] \geq v) \leq \exp(-v^2/2\sigma^2).$$

where $\sigma = 1$ in our case.
Setting $\exp(-v^2/2) \leq \alpha$ yields

$$v \geq \sqrt{2\log(1/\alpha)},$$

To achieve coverage at least $1-\alpha$, the radius must satisfy this bound (noting that the actual quantile may be smaller, but this provides a conservative estimate used for the universal threshold). □

Lemma 2. *The expected radius produced by $R_{\mathcal{Z}}(X)$ satisfies*

$$\mathbb{E}_X[v^k(X)] \leq \sqrt{\frac{2}{\pi}} + \bar{G},$$

where $\bar{G} = \mathbb{E}_X[G(X)]$ and $G(X) = v^k(X) - E(X)$.

Proof. Because the proposed APR algorithm generates the region $R_{\mathcal{Z}}(X)$ in a test-conditional way, for each realization of X, the quantile threshold and the region $R_{\mathcal{Z}}(X)$ are different. We analyze the expected radius, accounting for randomness over all possible realizations of X.

Denote $G(X) = v^k(X) - E(X)$ as the distance between $E(X)$ (the center in $\mathcal{Z}$ for X) and the adaptive quantile radius $v^k(X)$ determined by the k-NN of X in $\mathcal{Z}$. Let $\bar{G} = \mathbb{E}[G(X)]$. Recall that the PDF of a Gaussian distribution $\mathcal{N}(0,1)$ is $P(v) = \frac{\exp(-v^2/2)}{\sqrt{2\pi}}$. The expected value of the absolute deviation (folded normal) is relevant for the typical radius contribution:

$$\begin{aligned}
\mathbb{E}_X[v^k(X)] =& \mathbb{E}_X[E(X) + G(X)] \leq \mathbb{E}_X[E(X)] + \bar{G} \\
=& \int_0^\infty v \cdot \frac{2\exp(-v^2/2)}{\sqrt{2\pi}}\, dv + \bar{G} \\
\overset{(a)}{=}& 2 \cdot \frac{1}{\sqrt{2\pi}} \int_0^\infty \exp(-u)\, du + \bar{G} \\
=& \frac{2}{\sqrt{2\pi}} + \bar{G} = \sqrt{\frac{2}{\pi}} + \bar{G},
\end{aligned}$$

where (a) follows from the substitution $u = v^2/2$, so $du = v\,dv$. □

Combining Lemmas 1 and 2, if $\bar{G} \leq \sqrt{2\log(1/\alpha)} - \sqrt{2/\pi}$, then $\mathbb{E}_X[v^k(X)] \leq v$. This holds because $\bar{G}$ represents the expected additional margin due to variability in the k-NN estimates. Due to the concentration properties of Gaussian random variables in the ideally learned $\mathcal{Z}$ (where most mass is near the origin), the local k-NN samples exhibit low variability for sufficiently large k, bounding $\bar{G}$ sufficiently small to satisfy the inequality, as supported by the empirical results.

This implies

$$\mathbb{E}_X[|R_{\mathcal{Z}}(X)|] \leq \mathbb{E}_X[|R_{\mathcal{Z}}(X)|].$$

By the assumption that the decoder $\mathcal{D}$ preserves the relative order of the expected volume, we have

$$\mathbb{E}_X[|\mathcal{D}(R_{\mathcal{Z}}(X))|] \leq \mathbb{E}_X[|\mathcal{D}(R_{\mathcal{Z}}(X))|],$$

or equivalently,

$$\mathbb{E}_X[|R_{\mathcal{Y}}(X)|] \leq \mathbb{E}_X[|R_{\mathcal{Y}}(X)|].$$

□

A.2 Dataset Splits and Hyperparameter `k` for k-NN

This section provides further details about the number of data points used for training, testing, validation, calibration (for other methods), and average k calibration inputs (for both variants of APR) across all datasets. To choose k for the test input-conditioned quantile threshold in APR, we performed a systematic search within 30% to 90% of the calibration set(i.e., we sweep $k \in \{0.3m, 0.4m, \ldots, 0.9m\}$ with $m = |\mathcal{D}_{cal}|$) and report the best-performing k; we also observe stable behavior across a broad range of k values., selecting the k value that provides the smallest region size. d is the number of target outputs for each multi-target regression task.

Dataset	`Targets`	Training	Testing	Validation	Calibration	`mean k (%)`
BIWI_2	2	512	200	160	128	104.00(82.00%)
BIWI_3	3	512	200	160	128	104.00(82.00%)
Community_2	2	1020	399	319	256	180.15 (70.4%)
Community_3	3	1020	399	319	256	189.15 (73.9%)
Community_4	4	1020	399	319	256	203.25 (79.3%)
Bio	2	5120	2000	1600	1280	1100.80 (86.0%)
House	2	11065	4323	3458	2767	1259.75 (45.5%)
Blog	2	11264	4400	3520	2816	1239.10 (44.0%)
Maint._2	2	1024	400	320	256	152.80 (60.0%)
Maint._3	3	1024	400	320	256	168.15 (65.7%)
Maint._4	4	1024	400	320	256	141.20 (55.2%)

Table 5: Number of training, testing, validation, calibration (for other methods), the number of APR calibration points k (averaged over 20 runs) across all datasets.

A.3 Real Experimental Results

GitHub Repository. The code necessary for implementing APR and replicating the results of our paper can be found in the following anonymous GitHub repository: `https://anonymous.4open.science/r/apr-4C4C/`

Compute Machine Specifications: All experiments were conducted on the following hardware and software setup:

- **Operating System:** Rocky Linux 8.10 (Green Obsidian), **Processor:** AMD EPYC 7573X 32-Core Processor
- **GPUs:** Two NVIDIA A40 GPUs (each with 46 GB of memory), **GPU Driver Version:** 555.42.02, **CUDA Version:** 12.5

Coverage Rate and Relative Region Area in the Target Space $\mathcal{Y}$

Dataset	Targets	Methods	Coverage	Region Area ↓	Reduction(%) from Naive ↑	Reduction(%) from SOTA ↑
BIWI	3	Naive	0.92 (0.006)	521.92 (38.24)	–	–
		SOTA	0.91 (0.013)	352.69 (56.76)	32.42%	–
		APR-U	0.90 (0.013)	328.67 (51.18)	37.03%	6.81%
		APR-W	0.89 (0.013)	299.51 (46.15)	**42.61%**	**15.08%**
BIWI_3	3	Naive	0.93 (0.008)	12373.15 (1429.73)	–	–
		SOTA	0.92 (0.009)	5202.63 (951.92)	57.95%	–
		APR-U	0.91 (0.010)	4747.07 (941.92)	61.63%	8.76%
		APR-W	0.90 (0.010)	4049.22 (771.71)	**67.27%**	**22.17%**
Community_2	2	Naive	0.90 (0.004)	885.48 (26.13)	–	–
		SOTA	0.91 (0.005)	402.07 (12.48)	54.59%	–
		APR-U	0.89 (0.006)	378.31 (10.36)	57.28%	5.91%
		APR-W	0.89 (0.006)	375.74 (10.26)	**57.57%**	**6.55%**
Community_3	3	Naive	0.90 (0.006)	21933.56 (1050.76)	–	–
		APR-W	0.90 (0.007)	4394.57 (202.64)	77.94%	–
		SOTA	0.91 (0.005)	4838.51 (231.29)	79.65%	7.75%
		APR-U	0.90 (0.006)	4463.30 (206.48)	**79.96%**	**9.18%**
Community_4	4	Naive	0.90 (0.006)	35745.29 (2689.90)	–	–
		SOTA	0.91 (0.004)	3566.06 (292.63)	90.02%	–
		APR-U	0.90 (0.005)	3160.70 (214.17)	91.16%	11.37%
		APR-W	0.90 (0.005)	3082.39 (208.17)	**91.38%**	**13.56%**
Bio	2	Naive	0.90 (0.002)	504.75 (7.84)	–	–
		SOTA	0.90 (0.003)	432.41 (6.16)	**14.33%**	–
		APR-U	0.90 (0.003)	436.11 (6.31)	13.60%	-0.86%
		APR-W	0.90 (0.003)	435.61 (6.31)	13.70%	-0.74%
House	2	Naive	0.90 (0.002)	384.00 (5.08)	–	–
		SOTA	0.90 (0.002)	339.75 (8.73)	11.52%	–
		APR-U	0.89 (0.002)	326.75 (9.89)	14.91%	3.83%
		APR-W	0.89 (0.002)	326.23 (9.89)	**15.05%**	**3.98%**
Blog	2	Naive	0.90 (0.001)	245.15 (6.65)	–	–
		SOTA	0.90 (0.002)	259.81 (11.65)	-5.98%	–
		APR-U	0.87 (0.003)	218.82 (12.99)	10.74%	15.78%
		APR-W	0.87 (0.003)	216.41 (12.91)	**11.73%**	**16.71%**
Maint._2	2	Naive	0.90 (0.006)	466.12 (173.51)	–	–
		SOTA	0.99 (0.001)	147.27 (15.00)	68.41%	–
		APR-U	0.86 (0.009)	21.16 (1.45)	**95.46%**	**85.63%**
		APR-W	0.95 (0.005)	21.34 (1.44)	95.42%	85.51%
Maint._3	3	Naive	0.91 (0.006)	1213850.9 (408676)	–	–
		SOTA	0.98 (0.002)	3590.52 (752.77)	99.70%	–
		APR-U	0.88 (0.008)	2913.02 (712.51)	99.76%	18.87%
		APR-W	0.94 (0.006)	2493.11 (641.75)	**99.79%**	**30.56%**
Maint._4	4	Naive	0.91 (0.005)	53031241 (26324344)	–	–
		SOTA	0.98 (0.002)	5957.45 (1298.19)	99.99%	–
		APR-W	0.98 (0.006)	4277.23 (2066.71)	99.99%	28.20%
		APR-U	0.87 (0.010)	4282.11 (2066.65)	**99.99%**	**28.12%**

Table 6: Coverage rates, relative region size, and reduction in region size of APR relative to SOTA method in the latent space $\mathcal{Y}$ presented for nine datasets with multiple targets from different areas. Results for each dataset are averaged over 20 experimental runs with standard errors provided. Detailed raw experimental data are provided in Appendix A.3.

Coverage Rate and Region Area in the Target Space $\mathcal{Y}$

Dataset	Targets	Methods	Coverage	Reduction(%) Region Area ↓	Reduction(%) from Naive ↑	from SOTA ↑
Bio	2	Naive	0.94	715.83	–	–
		SOTA	0.95	596.02	16.74%	–
		APR-U	0.94	587.96	17.86%	1.35%
		APR-W	0.95	587.15	**17.98%**	**1.49%**
BIWI_2	2	Naive	0.97	1266.76	–	–
		SOTA	0.96	609.81	51.86%	–
		APR-U	0.94	526.68	58.42%	13.63%
		APR-W	0.93	487.22	**61.54%**	**20.10%**
BIWI_3	3	Naive	0.96	30841.33	–	–
		SOTA	0.96	7459.55	75.81%	–
		APR-U	0.95	7098.47	76.98%	4.84%
		APR-W	0.94	6036.01	**80.43%**	**19.08%**
Blog	2	Naive	0.95	475.96	–	–
		SOTA	0.96	404.87	14.94%	–
		APR-U	0.93	359.69	24.43%	11.16%
		APR-W	0.93	355.85	**25.24%**	**12.11%**
Community_3	3	Naive	0.96	55285.24	–	–
		SOTA	0.96	9890.66	82.11%	–
		APR-U	0.95	8832.62	84.02%	10.70%
		APR-W	0.95	8688.65	**84.28%**	**12.15%**
Community_4	4	Naive	0.95	92377.72	–	–
		SOTA	0.96	7520.86	91.86%	–
		APR-U	0.95	6904.66	92.53%	8.19%
		APR-W	0.95	6735.23	**92.71%**	**10.45%**
Community_2	2	Naive	0.96	1611.00	–	–
		SOTA	0.96	616.96	61.70%	–
		APR-U	0.95	575.77	64.26%	6.68%
		APR-W	0.95	571.18	**64.55%**	**7.42%**
House	2	Naive	0.95	554.69	–	–
		SOTA	0.95	457.18	17.58%	–
		APR-U	0.94	428.25	22.79%	6.33%
		APR-W	0.94	427.33	**22.96%**	**6.53%**
Maint._2	2	Naive	0.94	2045.03	–	–
		SOTA	0.99	169.80	91.70%	–
		APR-U	0.92	19.03	99.07%	88.79%
		APR-W	0.97	20.42	**99.00%**	**87.98%**
Maint._3	3	Naive	0.95	4187810.75	–	–
		SOTA	0.98	5419.40	99.87%	–
		APR-U	0.93	1278.50	99.97%	76.41%
		APR-W	0.97	1281.79	**99.97%**	**76.35%**
Maint._4	4	Naive	0.95	238938747.50	–	–
		SOTA	0.97	12328.73	99.99%	–
		APR-U	0.93	1279.99	100.00%	89.62%
		APR-W	0.99	1134.18	**100.00%**	**90.80%**

Table 7: Coverage rates, region area, and reduction in region size of APR relative to SOTA in $\mathcal{Y}$.